Multiphase Modeling of Hydrogen Production in Zero Gap Alkaline Water Electrolyzer

&

Self-Terminating Electrodeposition of Platinum on Gold for PEMFC Electrodes

A Project Report

submitted in fulfillment of the

requirements for the degree of

Master of Technology

in the Faculty of Engineering by

Sevalur Mahendran Prasanth

Department of Chemical Engineering

Indian Institute of Science

Bengaluru 560012 (India)

June 2023

Dedicated to

My Family

Declaration

I certify that the report was written by myself, and in writing the report,

1. The experimental, simulation, and Modelling results I obtained have been presented without bias, modifications, or alterations and can be obtained using the information provided in the report.
2. I have not copied material from published/unpublished sources (reports, textbooks, papers, websites, etc.)
3. Where material from any source was used, the source was given due credit by citing it in the text of the report and giving its details in the section on references, and
4. Where material from any source was copied, it was put in quotation marks, and the source was given due credit by citing it in the text of the report and giving its details in the section on references.

Signature of the author: .....

Prasanth Sevalur Mahendran

Department of Chemical Engineering

Indian Institute of Science, Bengaluru

Acknowledgment

I sincerely thank my adviser Dr. Venugopal Santhanam for his constant guidance and support throughout my project and my master's career. I also thank him for the immense freedom and insightful conversations that helped me learn and grow as a student and a researcher.

I am grateful to Dr. Abhineet Gupta and Dr. Shauvik De for their support and guidance during my research internship at SHELL Technology Center Bangalore. Their expertise in the "High fidelity multiphase modeling of hydrogenics in zero-gap alkaline water electrolyzer" project was invaluable. I appreciate their constant encouragement, insightful input, and dedication, significantly contributing to the project's success.

I would also like to thank all the department faculty members for making coursework enjoyable and training me for research. I also thank all the non-teaching staff for helping me with all the non-academic issues.

I want to thank all my friends at IISc who made my stay on the campus memorable

and the ones outside who continue to make their support felt despite the distance.

I thank my lab mates for their interactions and input during my stay at IISc.

Thanks to Khantesh, Adarsh, Nikita, Rupesh, Abhishek, and Armaan for all the brainstorming sessions and discussions.

Lastly, I thank my parents for their ongoing care, motivation, and patience throughout my academics.

Abstract

Electrolytic hydrogen production offers high energy density and long duration storage capabilities. Alkaline Water Electrolysis (AWE) stands out as a cost-effective and mature technology for hydrogen production. Traditional AWE suffers from high internal resistance, limiting operation to low current densities. The Zero Gap configuration of AWE (ZGAWE) overcomes this limitation by reducing ohmic overpotential and enabling higher current densities for improved efficiency. This study developed a 2D, 2Phase electrochemistry-transport coupled model of the ZGAWE cell using COMSOL Multiphysics. The model simultaneously solved fluid dynamics and electric current conservation equations, incorporating the Euler-Euler approach to describe the two-phase bubbly flow. Comparative studies were conducted between a standard non-zero gap alkaline electrolyzer and a zero gap alkaline water electrolyzer for the developed model, followed by experimental validation of the same parameters in accordance with the reported literature. In the second part, we investigated the electrodeposition of platinum on gold substrates for potential use in PEMFC electrodes. A specific electrolyte composition with pH four was employed, and linear sweep voltammetry and self-terminating electrodeposition techniques were utilized. Multiple studies examined pH variations, the influence of electrodeposition cycles, and the quantification of platinum deposition. The results showed stable pH throughout the process, regardless of cycle number, and reproducible deposition with 3-5 $\mu g/cm^2$ loading levels. These findings enhance our understanding of platinum-gold composites for optimizing PEMFC electrode performance and reliability.

Contents

List of Figures

List of Tables

Chapter 1

1. Introduction

The current era is marked by the formidable challenge of climate change, which calls for urgent measures to be taken in the energy sector. The growth of the world economy is propelled by two interrelated factors: population expansion and the relentless pursuit of enhanced personal comfort. However, the consequences of this growth have exerted substantial pressures on the current fossil fuel-based economic framework, characterized by a surge in greenhouse gas (GHG) emissions. As we strive towards a sustainable future, transitioning from fossil fuel-based energy systems to zero-carbon alternatives becomes paramount.

The International Energy Agency (IEA) presents compelling evidence, indicating a staggering increase in global energy consumption by 99.64% over a span of four decades (1975-2015)[1]. Correspondingly, carbon dioxide (CO_2) emissions have witnessed a substantial rise of 109% during this period. This alarming scenario has prompted the generation of comprehensive environmental impact studies and the formulation of policies aimed at safeguarding our environment on a global scale. Moreover, the non-renewable nature of fossil fuels and their uneven distribution across the globe have further contributed to geopolitical conflicts and socio-economic disparities.

Renewable energy sources, particularly wind and solar power, have emerged as promising solutions in this paradigm shift. However, a significant hurdle associated with these renewable

sources is their inherent intermittency, stemming from their dependence on weather conditions. This intermittency gives rise to a misalignment between energy supply and demand, potentially leading to grid instability and failures. Hence, developing and integrating reliable energy storage systems are critical as they enable the effective management of intermittent renewable energy sources[2].

1.1 Alkaline Water Electrolysis

In the quest for long-term storage solutions for renewable energies, chemical energy carriers have emerged as a promising avenue. Hydrogen has garnered significant attention among these carriers due to its inherent advantages. Its efficient production from surplus renewable energy through water electrolysis positions hydrogen as a compelling candidate for energy storage[3]. Notably, the utilization of hydrogen can be realized through various means, including transportation via a dedicated hydrogen distribution grid or integration into the existing natural gas grid[4]. Additionally, appropriate facilities enable the storage of hydrogen for future use. Notably, hydrogen can be seamlessly converted back into electricity through the utilization of fuel cells, facilitating its integration into the electricity grid. Furthermore, hydrogen exhibits versatility as a fuel in the transportation sector and holds potential for new industrial processes[5].

Electrolytic hydrogen generation processes have emerged as a promising technique for the long-term storage of renewable energies[6]. Hydrogen's versatility as an energy carrier is a notable

advantage, finding applications in electricity generation through fuel cells, as a reactant in chemical processes, and as a power source for automobiles. Alkaline water electrolysis (AWE) and proton exchange membrane water electrolysis (PEMWE) are the predominant technologies employed in industrial settings, with AWE exhibiting advantages in terms of robustness, cost, and system maturity. Although PEMWE offers superior performance, relying on noble metals, such as platinum (Pt), increases its cost[7]. In recent years, significant progress has been made in optimizing AWE, primarily focused on minimizing activation losses, reducing the cost of electrolyzers, and addressing electrode material selection. Moreover, researchers have explored using anion exchange membranes (AEMs) and zero-gap cell configurations to mitigate ohmic losses and enhance performance.

1.2 Self-Terminating Electrodeposition (STED) of Platinum on Gold for PEMFC Electrodes

Proton Exchange Membrane Fuel Cells (PEMFCs) have gained significant attention in recent years as promising alternative energy technology for various applications, including automotive, stationary power generation, and portable devices. PEMFCs offer several advantages over conventional energy sources, such as high energy efficiency, low emissions, and quiet operation. However, their widespread commercialization is hindered by several challenges, including the high cost and limited availability of platinum (Pt), which is a crucial catalyst material used in PEMFC electrodes[8]. To address the issue of high Pt loading in PEMFC electrodes, extensive

research has been focused on developing efficient Pt deposition techniques that can optimize Pt utilization while maintaining high catalytic activity. One such technique is Self-Terminating Electrodeposition (STED), which enables the controlled deposition of Pt on gold (Au) substrates to form Pt/Au composite electrodes with enhanced catalytic properties.

STED is a highly attractive method for Pt deposition due to its ability to achieve atomic monolayer coverage of Pt on Au substrates. The process involves the sequential application of specific potentials, where the Pt deposition potential is set to a value below the thermodynamic potential for complete Pt monolayer coverage, and the subsequent desorption potential is set above the potential required for hydrogen underpotential deposition (Hupd). This unique approach allows the electrodeposition process to self-terminate after achieving the desired Pt coverage, resulting in controlled and efficient Pt utilization[9,10].

The STED technique offers several advantages over traditional Pt deposition methods. Firstly, it enables the deposition of Pt at significantly reduced loading levels compared to conventional techniques, thereby minimizing Pt consumption and reducing overall cost. This is particularly crucial considering the limited availability and high cost of Pt. Secondly, the controlled deposition of Pt on Au substrates allows for the creation of well-defined catalytic sites with enhanced electrochemical performance and improved durability. The Pt/Au composite electrodes prepared using STED exhibit excellent catalytic activity, high current densities, and long-term stability, making them highly desirable for PEMFC applications[11].

Chapter 2

2.Literature Survey

2.1 Modeling Alkaline Water Electrolyzer

Alkaline water electrolysis is vital for large-scale hydrogen production using renewable energy. Optimizing each component of the hydrogen energy system is crucial to increase operation time and efficiency and make electrolysis competitive with fossil fuel-based methods. Conventional alkaline water electrolyzers face limitations in partial load range and with gas impurity, necessitating safety shutdowns and voltage optimization. Integration with photovoltaic panels and wind turbines requires suitable converters. Combining electrolysis with hydrogen storage and fuel cells stabilizes the power grid and reduces carbon emissions. Understanding and modeling system dynamics, impurity effects, and power conversion are key for efficient operation and decarbonization. Further research is needed to develop physically-based models and improve system descriptions for various designs [12].

Hydrogen storage is a promising technology for renewable energy resources but is hindered by its high cost. Electrocatalysts and Computational Fluid Dynamics (CFD)-assisted design are efficient methods to improve electrolyzers' efficiency. A two-phase hydrodynamics model was compared to experimental velocity profiles, showing good agreement. Introducing a new bubble transfer

phenomenon called "bubble diffusion" improved convergence and agreement with experimental data. However, grid resolution and 2D geometry limitations require further calculations and consideration of parameters like bubble radius and current density to enhance hydrodynamic characterization[13].

The hydrodynamic properties of gas-liquid flows in water electrolyzers significantly impact energy requirements for hydrogen production. Incorporating the turbulence dispersion force, drag, and buoyancy forces improved the accuracy of gas layer spreading predictions in the Euler-Euler model. User-defined functions were necessary for momentum balance. Selecting suitable CFD models remains unresolved, with many models lacking generality. The study emphasized the importance of turbulence dispersion force for simulating gas-liquid flow and achieved qualitative agreement with experimental data, it was mentioned that research should focus on validating the Eulerian model at high gas volume fractions using detailed experimental data [14].

The reported model in [15] successfully simulated the fluid dynamic and electrochemical phenomena in an AWE cell and achieved a good fit with experimental data, with less than 1% error for polarization curves. The model analyzed the effects of temperature, electrode-diaphragm distance, and electrolyte conductivity on the cell's electrical response and gas profiles. The model demonstrated improved performance at higher temperatures, smaller electrode-diaphragm distances, and higher electrolyte conductivity. However, further investigations are needed to study the charge transfer coefficient and the zero-gap cell design to enhance the accuracy and applicability of the model in real industrial-sized electrolyzer systems[15].

A three-dimensional numerical model was developed considering the quantitative relationship between electrochemical and fluidic processes in industrial AWE cells. The model incorporates the structural design of AWE equipment, addressing the shunting current effect. Results show that considering bubble effects, the Multiphysics model accurately predicts the current-voltage characteristic curve with less than 5% relative error. The model provides insights into the interaction between two-phase flow and electrochemical processes, emphasizing the importance of uniform current density distribution and structural improvements. The developed model facilitates quantitative optimization of AWE cell design, bridging the gap between research and industrial manufacturing [1].

The primary objective of this study is to create a Multiphysics model that integrates two-dimensional, two-phase electrochemistry transport. The study aims to develop a zero-gap alkaline water electrolyzer, a relatively underexplored area in the current research literature. The model will be utilized to analyze the electrochemical response through polarization curves and evaluate the overpotential reduction.

2.2 Self-Terminating Electrodeposition (STED) of Platinum on Gold for PEMFC Electrodes

STED enables the electrodeposition of atomic-scale platinum overlayers under ambient conditions. STED employs a double pulse voltametric approach and offers scalability and additivity in the deposition process. Notably, STED can be considered equivalent to liquid-phase atomic layer deposition (ALD). Unlike typical vapor-phase ALD methods, STED exhibits superior speed due to its reliance on cyclic modulation of the electrode potential instead of reactant exchange for each layer formation. One of the notable advantages of STED is its ability to provide precise control over platinum loading by repeating the voltage cycle, allowing for the deposition of the desired number of platinum overlayers. This level of control is crucial in tailoring the properties and thickness of platinum films for specific applications. The introduction of STED as an electrodeposition technique for atomic-scale platinum overlayers presents a significant advancement in the field. Future investigations should optimize STED parameters, explore their applicability to other materials, and study potential synergies with existing deposition methods, as reported in the literature[10]. The deposition of platinum atomic overlayers using Self-Terminating Electrodeposition (STED) has exhibited remarkable potential in a wide range of contemporary reactions. Notably, these reactions include the hydrogen evolution reaction [16,17], hydrogen oxidation reaction [9], oxygen reduction reaction [18], and methanol/formic acid oxidation[19]. In recent studies [16,17], the STED-deposited platinum atomic overlayers have demonstrated enhanced catalytic performance. These overlayers' unique atomic-scale structure and controlled

deposition contribute to their favorable reactivity. These findings are significant in advancing catalytic processes of contemporary interest, offering opportunities for efficient energy conversion and fuel cell applications.

Previous studies have demonstrated the layer-by-layer atomic deposition of platinum using the self-terminating electrodeposition method and have shown the durability of platinum overlayers formed through this technique. Further, this study specifically aims to determine the influence of pH on the electrodeposition process and conduct repeatability studies of electrodeposition.

Chapter 3

3 Modeling Alkaline Water Electrolyzer

Water electrolysis is a process that involves splitting water molecules into hydrogen and oxygen gases using an electrical current. It occurs in an electrolytic cell, where two electrodes, typically made of metals like platinum, are immersed in a water-based electrolyte solution. When an electric voltage is applied across the electrodes, water molecules undergo a series of chemical reactions. At the anode, water molecules lose electrons, forming oxygen gas. At the cathode, water molecules gain electrons, forming hydrogen gas, as shown in Figure 1.

Alkaline water electrolysis is a widely recognized and established industrial procedure for generating hydrogen gas. Within the cell, the cathode facilitates the formation of hydrogen gas, while the anode facilitates the formation of oxygen gas. The electrolyte employed in this process is a liquid containing water, and the presence of gas bubbles formed during the reaction leads to a decrease in the effective ionic conductivity. Consequently, generating gases can adversely affect the cell's performance, primarily by reducing the accessible surface area for the electrode reactions. Figure 1 illustrates the configuration of an alkaline electrolysis cell. The cell consists of two electrodes, the anode, and the cathode, both immersed in a potassium hydroxide (KOH) aqueous solution serving as the electrolyte. These electrodes are separated by a porous diaphragm, which

permits the transport of hydroxide ions (OH^-) while preventing the passage of gases.

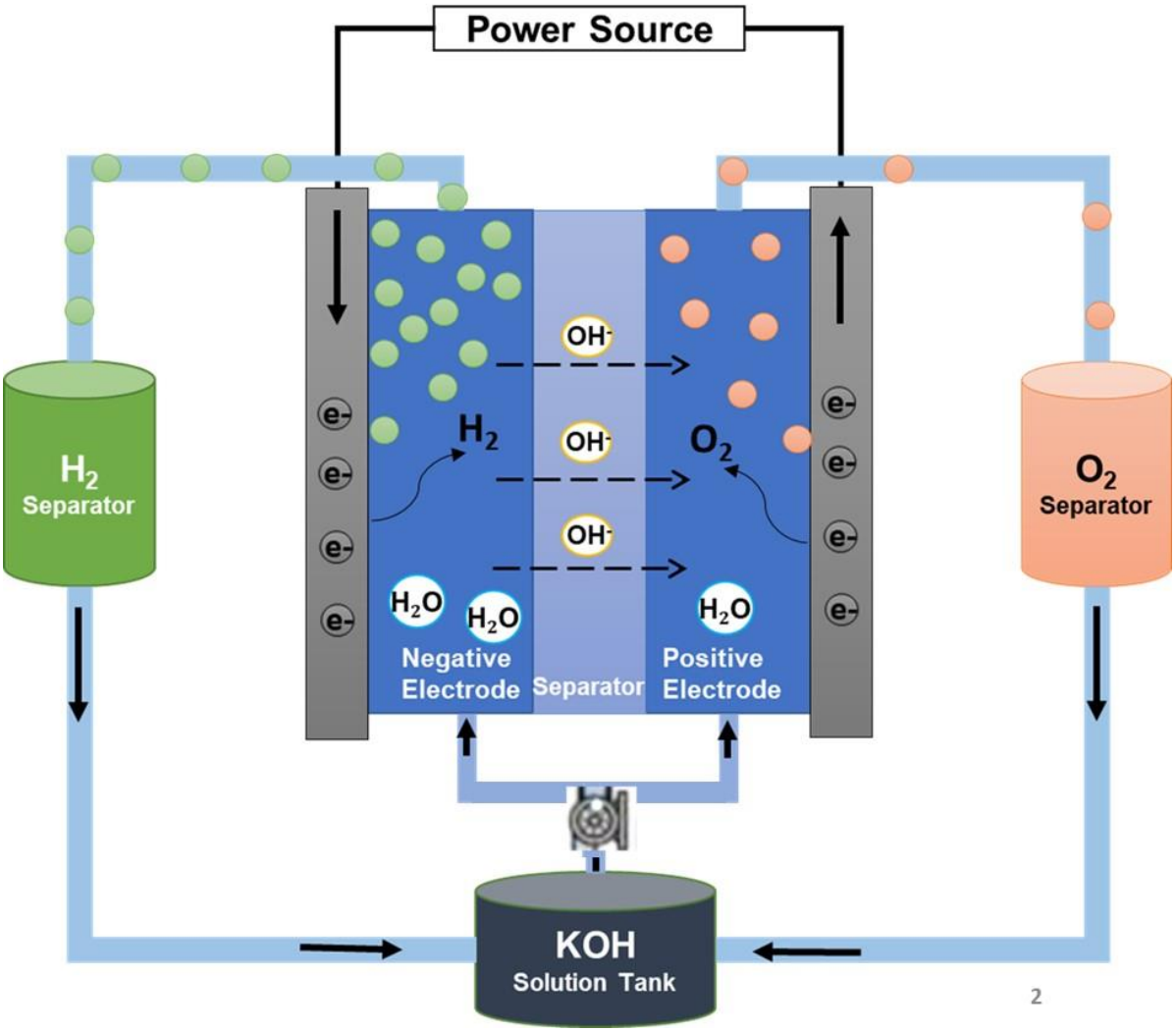

FIGURE 1 GENERAL SCHEME OF THE ALKALINE ELECTROLYSIS CELL.

During the typical operation of an electrolysis system, the electrolyte enters the anodic and cathodic compartments through the lower inlets. At the anode, an electrochemical reaction takes place, resulting in the generation of oxygen bubbles. Similarly, at the cathode, hydrogen is produced through another electrochemical process. As the electrolysis continues, these gas bubbles grow in size until they reach a critical size where they detach from the surface of their respective

electrodes. This detachment is facilitated by factors such as buoyancy and the accumulation of gas near the electrode surface. Once detached, the mixture of generated gases and electrolyte exits each compartment through the upper outlets, completing the cycle of gas evolution in the electrolysis process.

3.1 Electrochemistry

The alkaline electrolysis cell enables the splitting of water through the following overall reaction:

$$H_2O \rightarrow H_2 + \frac{1}{2}O_2$$

To initiate this reaction, an applied potential is required between the electrodes. Simultaneously, two half-cell reactions occur at the cathode and anode: the hydrogen evolution reaction (HER) at the cathode and the oxygen evolution reaction (OER) at the anode.

CATHODE (HER): $2\,H_2O + 2e^- \rightarrow H_2 + 2OH^-$ $E^{0,\,HER}$ = - 0.829 V vs SHE

ANODE (OER): $2\,OH^- \rightarrow \frac{1}{2}O_2 + H_2O + 2e^-$ $E^{0,\,OER}$ = + 0.401 V vs SHE

Reversible cell voltage (U_{rev}): refers to the potential difference required to drive an electrochemical reaction in an electrolytic cell under ideal reversible conditions. It represents the minimum voltage necessary to overcome the thermodynamic energy differences associated with electrolysis, ensuring the desired electrochemical decomposition occurs. In the case of water electrolysis under standard conditions (1 bar and 25 °C), the reversible cell voltage (U_{rev}) can be calculated as the difference between $E^{0,\,OER,}$ and $E^{0,\,HER}$

$$U_{rev} = E^{0,\,HER} - E^{0,\,OER}$$

$$U_{rev} = -1.23\ V$$

3.2 Thermodynamics

At standard conditions, according to the second law of thermodynamics

$$\Delta_R G = \Delta_R H - T\Delta_R S$$

Total change Gibbs free energy $\Delta G^o = 273.2\ kJ/mol$ This is in accordance with the equation.

$$U_{rev} = -\frac{\Delta G}{zF}$$

Thermoneutral Voltage (U_{th}): In electrochemistry, a thermoneutral voltage refers to the voltage drop across an electrochemical cell that facilitates the cell reaction and supplies the required heat to maintain a constant temperature. This phenomenon ensures thermodynamic equilibrium within the system.

$$U_{th} = -\frac{\Delta H}{zF}$$

U_{th} = -1.48 V

The real cell voltage (U) exceeds the reversible voltage due to irreversibilities or overpotentials. Hence, the real cell voltage can be defined as the combined value of reversible voltage and overpotentials (η).

$$U = Urev + \sum \eta$$

The total overpotential is the sum of individual activation (η_{act}), ohmic (η_{ohm}), and concentration overpotentials (η_{conc}).

$$\sum \eta = \eta_{act} + \eta_{ohm} + \eta_{conc}$$

Activation overpotentials: η_{act}

Activation overpotentials arise from the activation energies required for the formation reactions of hydrogen and oxygen on the electrode surfaces. These reactions involve the conversion of reactants into products. The activation energy represents the energy barrier that reactant molecules must overcome to participate in the electrochemical reaction. At lower temperatures or high reaction rates, the activation energy becomes a significant factor. Higher activation energies result

in higher activation overpotentials, causing a difference between the real and reversible cell voltages.

Ohmic overpotentials: η_{ohm}

Ohmic overpotentials are the result of electrical resistance within the cell components. This resistance can be attributed to several factors. The electrodes and current collectors possess electrical resistance due to their inherent material properties and geometry. Additionally, transport resistance contributes to Ohmic overpotentials. Gas bubbles formed during the electrochemical reactions can impede the flow of electrons, leading to increased resistance. Ionic transfer in the electrolyte can also encounter resistance, with bubbles hindering the movement of ions. Furthermore, the resistivity of the diaphragm or separator, which separates the reactants while transporting OH^- ions between the two chambers, also contributes to Ohmic overpotentials. The cumulative effect of these resistances leads to a drop in voltage along the cell, resulting in a higher real cell voltage compared to the reversible voltage.

Concentration overpotentials: η_{conc}

Concentration overpotentials arise due to limitations in mass transport at high current densities. When the current density increases, the consumption or production of reactants at the electrode surface can lead to concentration gradients near the electrode. These concentration gradients hinder the efficient diffusion or transport of reactants to and from the electrode surface, thus impeding

the reaction kinetics. This results in an additional overpotential known as concentration overpotential. Concentration overpotentials are particularly significant in systems where the reactants or products are involved in slow or limited diffusion processes.

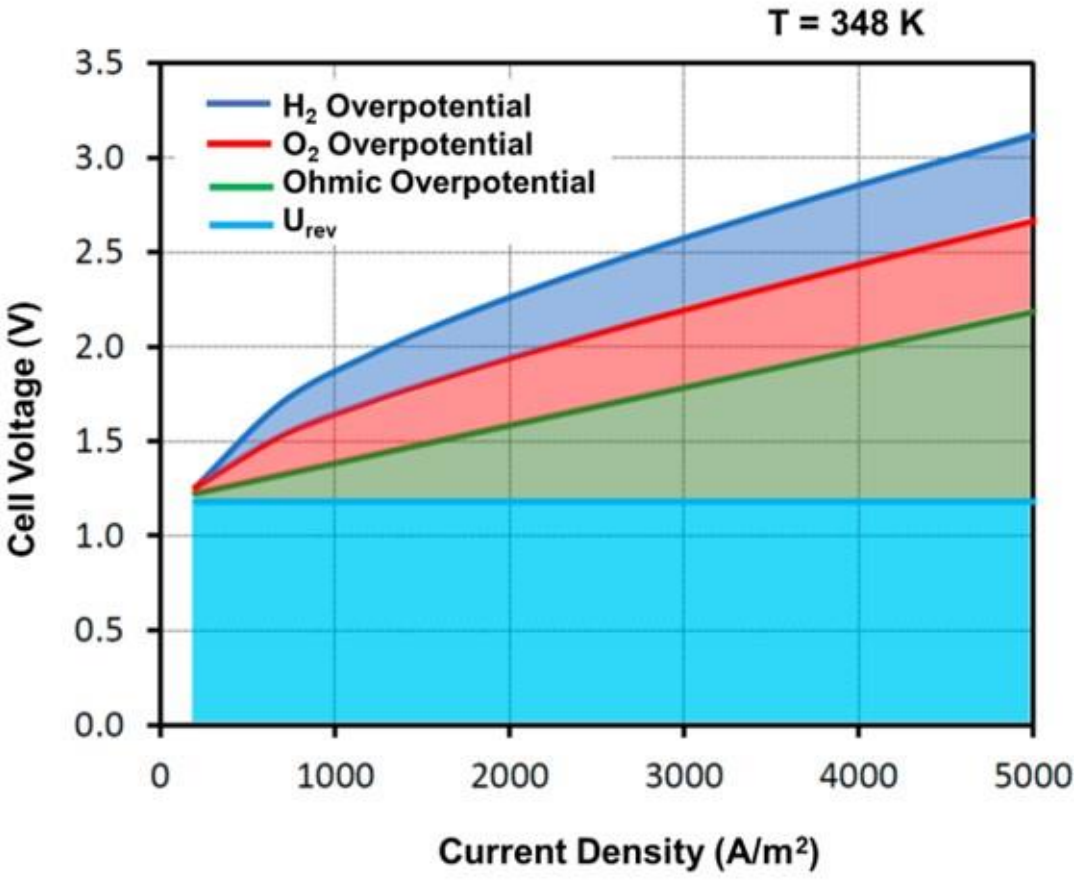

FIGURE 2 CONTRIBUTION OF EACH OVERPOTENTIAL IN *THE* POLARIZATION CURVE*[8].*

In summary, activation overpotentials result from the high activation energies required for reactions, Ohmic overpotentials stem from electrical and transport resistances within the cell components, and concentration overpotentials occur due to mass-transport limitations. These overpotentials collectively contribute to the deviation of the real cell voltage from the reversible voltage. Understanding and minimizing these overpotentials is crucial for optimizing the efficiency and performance of electrochemical cells and devices.

3.3 Model Geometry

Following Figure 1, a conventional alkaline water electrolysis cell consists of two compartments, each separated by a diaphragm or predominantly known as the membrane. The cathodic chamber serves as the site for the reduction of water to generate hydrogen gas, while the anode facilitates the oxygen evolution reaction to generate oxygen gas.

The diaphragm prevents gas mixing while maintaining a low ionic resistivity. To ensure compliance with fluid dynamic requirements, the model's geometry was constructed based on a rectangular small, scaled laboratory electrolysis cell. Simplifications were introduced to reduce the complexity of the model, resulting in a 2D geometry, as depicted in Figure 3. This simplification of the model was done to one-to-one comparison with experimental results and published model results in the reported literature models and further develop the zero-gap alkaline water electrolyzer model.

The electrode surfaces, with a height of 0.033 m, were represented by two simple boundary conditions Figure 3 applied on both sides of the cell. These regions act as current collectors where the desired potential is applied. Introducing these boundary conditions allows for analyzing electrochemical reactions occurring at the electrodes.

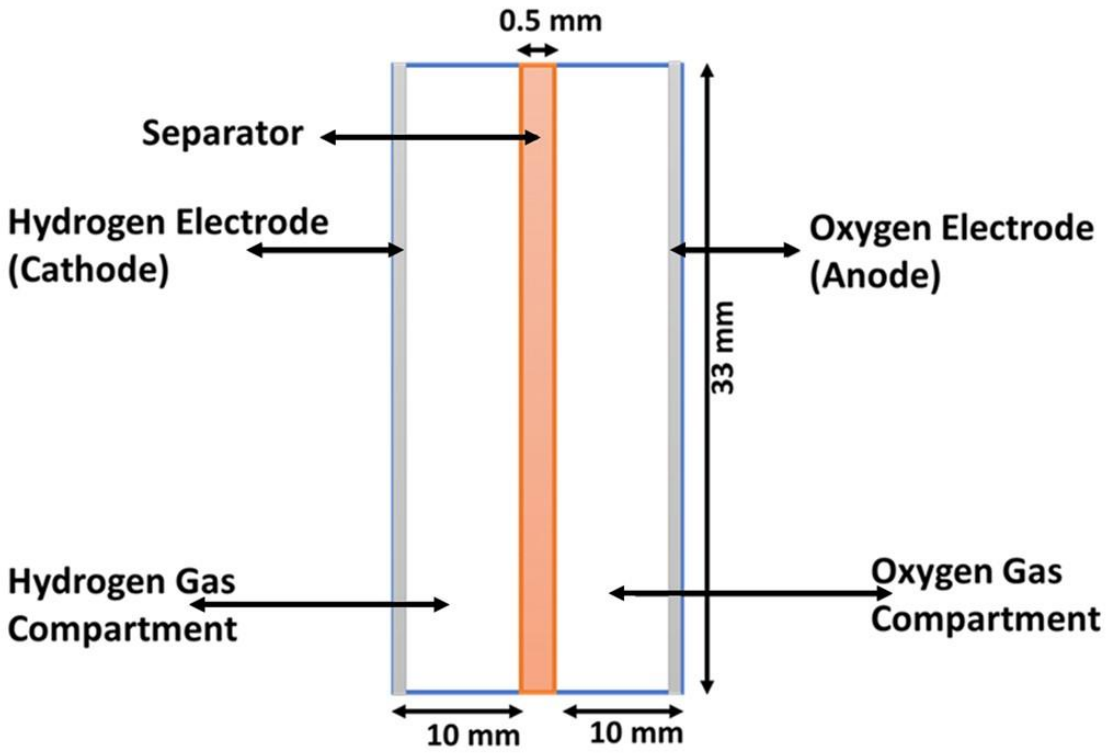

FIGURE 3 DEPICTION OF AN ALKALINE ELECTROLYSIS CELL.

The separator in Figure 3 was incorporated into the model's geometry as a thin rectangle with a thickness of 0.5 mm, effectively dividing the cell into the anodic and cathodic compartments. The separator is designed to enable the passage of ions while preventing the mixing of gases. In this

case, the separator permits only ionic conductivity, ensuring proper ion transport between the compartments.

The anodic (Oxygen gas compartment) and cathodic compartments (Hydrogen gas compartment) in Figure 3 were defined as two thick rectangles positioned between the separator and the corresponding electrode. The thickness of these compartments can vary depending on the specific model, with options of 1.5 mm, 4 mm, or 10 mm. The electrolyte inlet is located at the bottom of the compartments, facilitating the controlled introduction of the electrolyte. On the other hand, the outlet for the biphasic mixture of electrolyte and gases is positioned at the top, allowing for the removal of the evolved gases while maintaining proper electrolyte circulation.

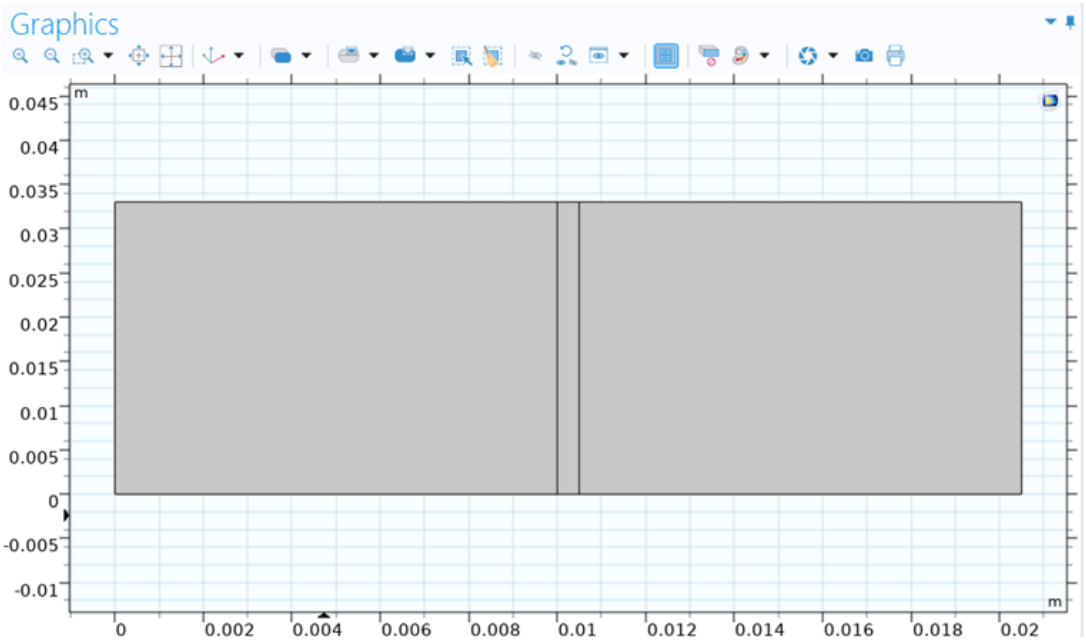

FIGURE 4 2D ALKALINE ELECTROLYSIS CELL COMSOL MODEL

By adopting this geometric configuration, the model provides a suitable approximation for studying alkaline water electrolysis. The 2D geometry allows for a detailed examination of fluid dynamics, mass transport phenomena, and electrochemical reactions occurring within the cell.

TABLE 1 PARAMETERS FOR 2D ALKALINE ELECTROLYSIS CELL COMSOL MODEL

Parameter	**Value**	**Unit**	**Description**
W_{H2}	10	mm	Hydrogen compartment width
W_{sep}	0.5	mm	Separator width
H_{cell}	33	mm	Cell Height
W_{O2}	10	mm	Oxygen compartment width
$d_{e\text{-}m}$	10	mm	NZG AWE Electrode-Diaphragm distance
F	96485	C	Faraday Constant
E_{cell}	5	V	Cell Voltage
$i_{0Cathode}$	21.1	A m^{-2}	Exchange Current Density
i_{0Anode}	1.1	A m^{-2}	Exchange Current Density
M_{H2O}	18	$gmol^{-1}$	Water Molecular Weight
$M_{OH\text{-}1}$	17	$gmol^{-1}$	Hydroxide Molecular Weight
M_{H2}	2	$gmol^{-1}$	Hydrogen Molecular Weight
M_{O2}	32	$gmol^{-1}$	Oxygen Molecular Weight

P	1	atm	Gas Pressure
T	303.15- 343.15	K	Cell Temperature
d_{bubble}	50	μm	Diameter of bubble
V	0.1	ms^{-1}	Average inlet velocity
epssep	0.55		Separator Porosity
C_{KOH}	5-10	M	Electrolyte Concentration

The imposed boundary conditions on the electrode surfaces simulate the behavior of current collectors, enabling the application of the desired potential and analyzing the electrode reactions. With its selective ionic conductivity, the thin rectangular separator ensures the separation of the anodic and cathodic compartments while facilitating the transport of ions. It plays a critical role in preventing gas crossover, which could adversely affect the overall cell performance. The defined dimensions of the anodic and cathodic compartments of the electrolyte inlet and biphasic mixture outlet promote efficient mass transport and gas removal within the cell. The geometric configuration optimizes the flow patterns, ensuring proper electrode and electrolyte interaction, thereby facilitating the desired electrochemical reactions.

In conclusion, based on a rectangular laboratory setup, the electrolysis cell model's presented geometric configuration provides a simplified yet comprehensive platform for studying alkaline water electrolysis. Adopting a 2D geometry, along with the defined electrode, separator, and

compartment dimensions, allows for a focused investigation of fluid dynamics, mass transport phenomena, and electrochemical reactions. While the model disregards certain three-dimensional effects, it remains valuable in understanding the fundamental aspects of the system and optimizing.

3.4 Initial and Boundary Conditions

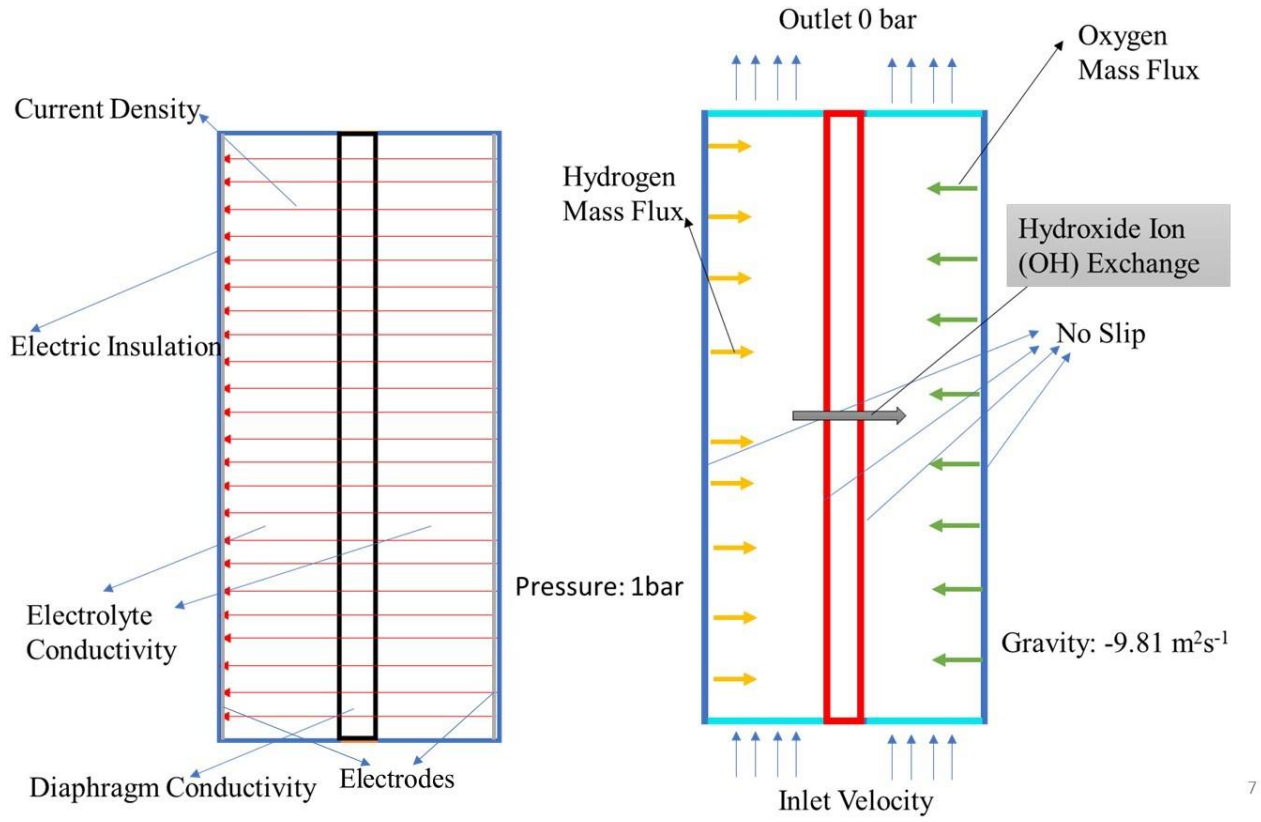

FIGURE 5 INITIAL AND BOUNDARY CONDITIONS FOR STD. ALKALINE WATER ELECTROLYZER MODEL.

In the fluid dynamics modeling of an electrolyzer, specific boundary conditions were employed to simulate the hydrogen and oxygen mass flux. The cathode and anode surfaces were assigned hydrogen and oxygen mass flux boundary conditions, respectively. For the separator, a hydroxide ion crossover boundary condition was specified. Inlet and outlet fluid flow boundary conditions

were imposed to ensure continuous fluid flow. Moreover, a no-slip boundary condition was applied to the walls of the electrolyzer, ensuring zero velocity at the wall boundaries.

In the electrochemical modeling, complete electric insulation was maintained on the walls of the electrolyzer. An electric field was established with a ramp function featuring a defined voltage at the anode and zero voltage at the cathode. Consequently, the electric field propagated from the anode to the cathode. The electrical conductivity was determined by correlating it with the temperature and electrolyte concentration inputs, employing the correlation equation of the electrolyte mentioned in the ohmic overpotential section.

3.5 Mesh

For the 2D alkaline electrolysis cell model in COMSOL, the meshing of the control domain was performed by generating a rectangular mesh. This approach capitalized on the inherent regularity of the cell's geometry, ensuring an efficient and accurate representation of the system.

Three distributions were created for the whole control domain.

TABLE 2 MESH DISTRIBUTIONS FOR THE ALKALINE WATER ELECTROLYZER MODEL

Distribution	Domain	No of Elements
Distribution 1	Electrode Surface Membrane Walls	500
Distribution 2	Inlet and Outlet	20
Distribution 2	Non-active surface of the membrane	6

A study on mesh independence was performed to determine the optimal number of nodes and elements for accurate simulations in the model. In the anode and cathode chambers, a maximum element size of 0.5 mm was used to capture the important characteristics of these regions. However, the element size was reduced to 0.01 mm near the walls to account for finer details. As the electrode-diaphragm distance varied from 0.01 m to 0.0015 m, the element sizes in the mesh were adjusted accordingly to maintain a consistent resolution and adapt to the changing distances. By employing smaller element sizes near the walls, the model was able to capture the complexities and phenomena occurring in these regions accurately. The mesh independence study allowed for identifying the optimal node and element configurations that provided reliable and converged results. By systematically varying the mesh density and assessing its impact on the simulation

outcomes, we ensured that the chosen mesh sizes achieved the desired balance between computational efficiency and accuracy.

3.6 Computational Fluid Dynamics Modelling

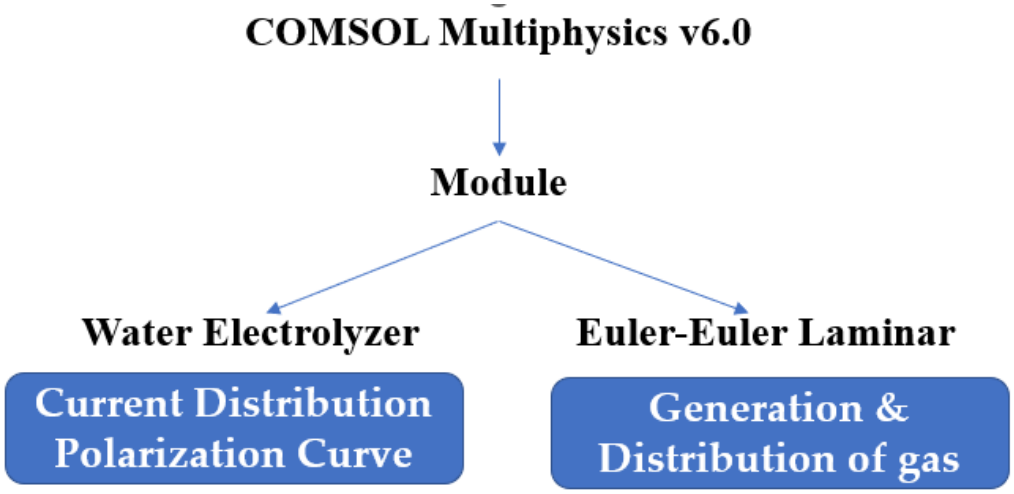

FIGURE 6 SCHEMATIC OF ALKALINE ELECTROLYZER MODELING

The alkaline electrolyzer was modeled using COMSOL Multiphysics with two fundamental modules: the Water Electrolyzer module and the Euler-Euler laminar module was selected to make the model simplified to develop a zero gap configuration. The Water Electrolyzer module was utilized to solve the current distribution and ensure the electrochemical reactions occurring at the defined electrode surface. To validate the electrochemical phenomena, polarization curves were generated.

On the other hand, the Euler-Euler laminar module was employed to address the fluid dynamics and describe the movement of gases and liquid. This module calculates the volume fraction occupied by each phase without intricate bubble details, providing a macroscopic model for two-phase fluid flow. It considers the two phases as interpenetrating media and tracks the average concentration of the phases. Each phase is associated with a velocity field, and their dynamics are described by momentum balance and continuity equations. Several simplifications are applied in this module. Firstly, the gas density is considered negligible compared to the liquid density. Secondly, the motion of gas bubbles relative to the liquid is determined by a balance between viscous drag and pressure forces. Lastly, the two phases share the same pressure field. In this simulation, a high level of bubble definition was not required, allowing for a reduction in computational cost while still providing a good approximation of the system.

Three solvers were employed for the analysis: the Stationary solver, the Current Initialization solver, and the Time-dependent solver. The differential equation was solved using the implicit backward differentiation method with a fixed tolerance of 0.001.

For time-dependent studies, the continuity equation is expressed as follows:

$$\nabla \cdot \vec{J} = Q_j \Rightarrow -\nabla \cdot \left[\sigma(\nabla U) - \frac{\partial \vec{D}}{\partial t} - \vec{J}_e\right] \cdot d = Q_j \cdot d$$

Where the variables are Current Density (J): A/m^2 , Electric Potential (U): V, Electrical Conductivity(σ): S/m, Current Source (Q): A/m^3, External Current Density (Je): A/m^2, Electric Displacement ($\frac{\partial \vec{D}}{\partial t}$): A/m^2 , Displacement (d): m.

Momentum Equation:

$$\Phi_l \cdot \rho_l \cdot \frac{\partial \vec{u}_l}{\partial t} + \Phi_l \cdot \rho_l \cdot (\vec{u}_l \cdot \nabla)\vec{u}_l$$
$$= -\nabla p + \nabla \cdot \left[\Phi_l \cdot (\psi_l) \cdot \left(\nabla \vec{u}_l - \frac{2}{3} \cdot (\nabla \overrightarrow{u_l}) \cdot \vec{I}\right)\right] + \Phi_l \cdot \rho_l \cdot \vec{g} + \vec{F}$$

Continuity Equation:

$$\frac{\partial}{\partial t}\left(\Phi_l \cdot \rho_l + \Phi_g \cdot \rho_g\right) + \nabla \cdot \left(\Phi_l \cdot \rho_l \cdot \vec{u}_l + \Phi_g \cdot \rho_g \cdot \vec{u}_g\right) = 0$$

In addition to the momentum equation for the liquid phase, the Euler-Euler Laminar module also includes a transport equation that describes the evolution of the volume fraction of the gas phase as follows:

$$\frac{\partial \Phi_g \cdot \rho_g}{\partial t} + \nabla \cdot \left(\Phi_g \cdot \rho_g \cdot \vec{u}_g\right) = -\dot{m}_{gl}$$

The fluxes of gases generated for Hydrogen H_2 and Oxygen O_2 on the active surfaces of electrodes are defined by the Faraday equation:

$$\dot{m}_{H2} = \frac{M_{H2}}{2 \cdot F} \cdot i$$
$$\dot{m}_{O2} = \frac{M_{O2}}{4 \cdot F} \cdot i$$

Where the variables are Velocity (u): m/s, Pressure (p): pa, Phase Volume Fraction (Φ): 1, Gravity Factor (g): m/s^2, Additional Volume Force (F): N/m^3, Dynamic Viscosity (Ψ): pa.s, Mass Transfer Rate gas-liquid ($\dot{m}_{gl}$): g/m^3.

3.7 Polarization Curve

The electrochemical response of the model was verified by generating polarization curves, which depict the relationship between voltage and current density.

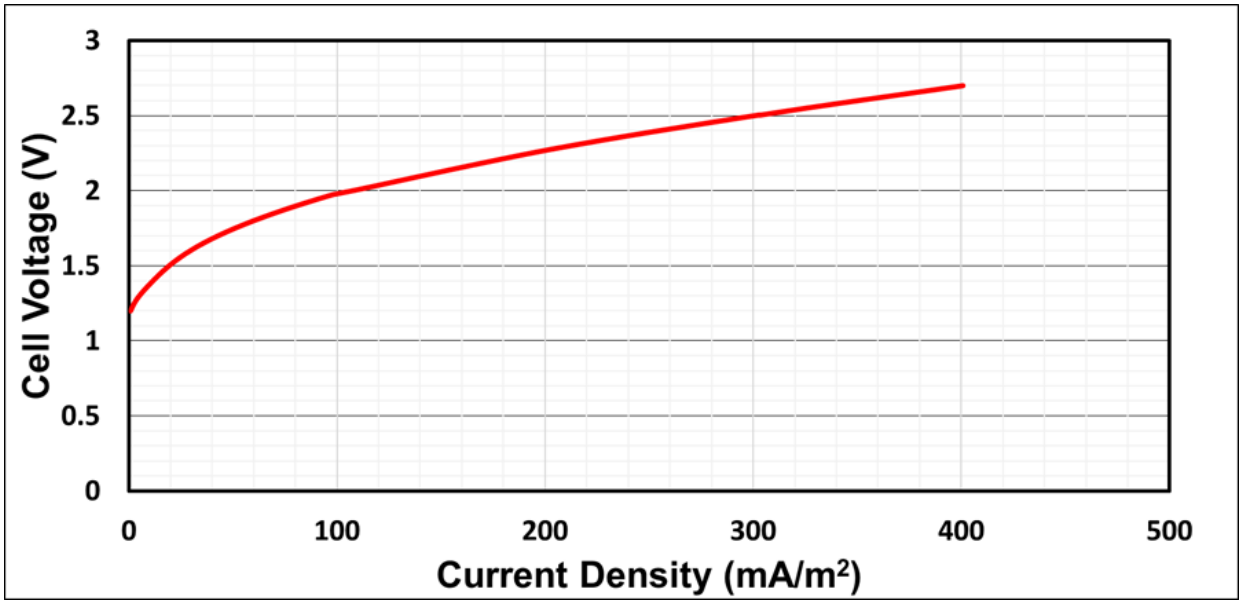

FIGURE 7 POLARIZATION CURVE AT CELL TEMPERATURE 50 °C AT 7.5 M (32 WT.%) KOH, 10MM ELECTRODE DISTANCE.

These curves serve as a means of validating the accuracy and reliability of the model's predictions. Polarization curves were constructed to validate the electrochemical response by varying the current density and measuring the corresponding voltage. This process involved systematically increasing the current density while recording the voltage values at each point. The resulting curve

illustrates how the voltage changes in response to different current density levels. The accuracy and fidelity of the model can be evaluated by comparing the generated polarization curves with experimental or theoretical data from the reported works of literature. As the model's polarization curve aligns with the reference data, the greater the confidence in the model's ability to accurately capture the electrochemical behavior of the system. The validation process involves not only the overall shape and trends of the polarization curve but also specific features such as the onset potential, limiting current density, and other characteristic points.

The following studies were conducted to assess the performance of the model:

1) Standard Non-Zero Gap Alkaline Electrolyzer: A conventional alkaline electrolyzer with a non-zero gap between the electrodes was simulated in this study. The polarization curve was generated by varying the current density and measuring the corresponding voltage. This curve serves as a baseline for comparison with other configurations.

2) Zero Gap Alkaline Electrolyzer: A zero gap configuration was simulated to investigate the effects of reducing the electrode gap. This configuration assumes that the electrodes are just separated by the membrane. The polarization curve for the zero-gap electrolyzer was generated by varying the current density and measuring the resulting voltage.

Comparative Studies between Non-Zero Gap and Zero Gap Alkaline Electrolyzer: A comparative analysis was performed to assess the differences in performance between the non-zero gap and

zero gap configurations. A direct comparison of their electrochemical responses can be made by plotting the polarization curves for both configurations. This comparison allows for evaluating the advantages and disadvantages of each configuration in terms of voltage requirements and current density.

Standard Non-Zero Gap Alkaline Electrolyzer

3.7.1 Influence of Cell Temperature

The polarization curves obtained from the current COMSOL model were compared to experimental data reported in a referenced research publication [15] under varying cell temperatures. The objective was to evaluate the agreement between the model's predictions and the experimental findings.

Consistent with expectations, the analysis revealed a decrease in the cell potential at a given current density as the temperature increased within the studied temperature range (Figure 8). Figure 8 provides empirical evidence showcasing the level of correlation between our model, experimental data, and the reported model from [15]. This behavior can be attributed to the positive influence of higher temperatures on the reaction kinetics, reducing the reversible voltage and consequently lowering the energy requirements for the alkaline electrolysis cell.

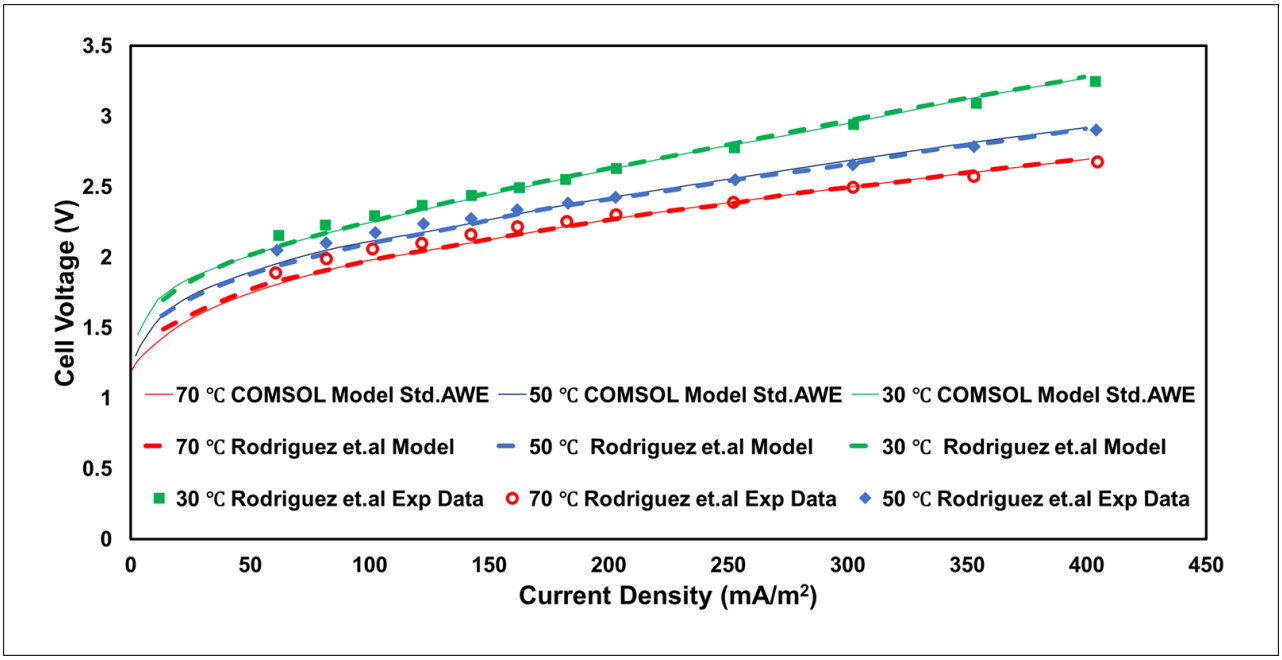

FIGURE 8 STANDARD NON-ZERO GAP ALKALINE ELECTROLYZER: POLARIZATION CURVE VARIATION AT DIFFERENT CELL TEMPERATURES (30-70) °C AT 7.5 M (32 WT.%) KOH, 10MM ELECTRODE DISTANCE WITH REFERENCE TO [15].

Notably, the strongest agreement among these datasets was observed at temperatures of 30 °C, 50 °C, and 70 °C. The observed correlation between the model's predictions and the experimental and calculated results at these specific temperatures underscores the model's capability to accurately capture the behavior of the alkaline electrolysis cell under varying temperature conditions. Such validation increases confidence in the model's reliability and its value for studying the impact of temperature on electrolysis system performance.

3.7.2 Influence of Electrolyte Concentration

The conductivity of the electrolyte plays a crucial role in determining the ohmic overpotential in the electrolysis cell. An empirical correlation for the conductivity of electrolyte (KOH) with concentration (w) and temperature (T) of the cell:

$$\sigma_{electrolyte} = -204.1 \cdot w - 0.28 \cdot w^2 + 0.5332 \cdot (w \cdot T) + 20720 \cdot \frac{w}{T} + 0.1043 \cdot w^3 - 0.00003 \cdot (w^2 \cdot T^2)$$

The Bruggeman equation below relates the effective conductivity of an electrolyte to the void phase fraction, which represents the volume occupied by voids or gas bubbles in the electrolyte[20]. The equation is given by:

$$\sigma_{eff-electrolyte} = \sigma_{electrolyte} \cdot \left(1 - \Phi_g\right)^{1.5}$$

The Bruggeman equation quantifies the reduction in conductivity caused by the presence of voids or gas bubbles in the electrolyte. As the void phase fraction increases, the effective conductivity decreases.

The above equations describe the importance of assessing the ohmic losses in the electrolyte and those associated with the diaphragm and gas bubbles generated in both the cathodic and anodic compartments.

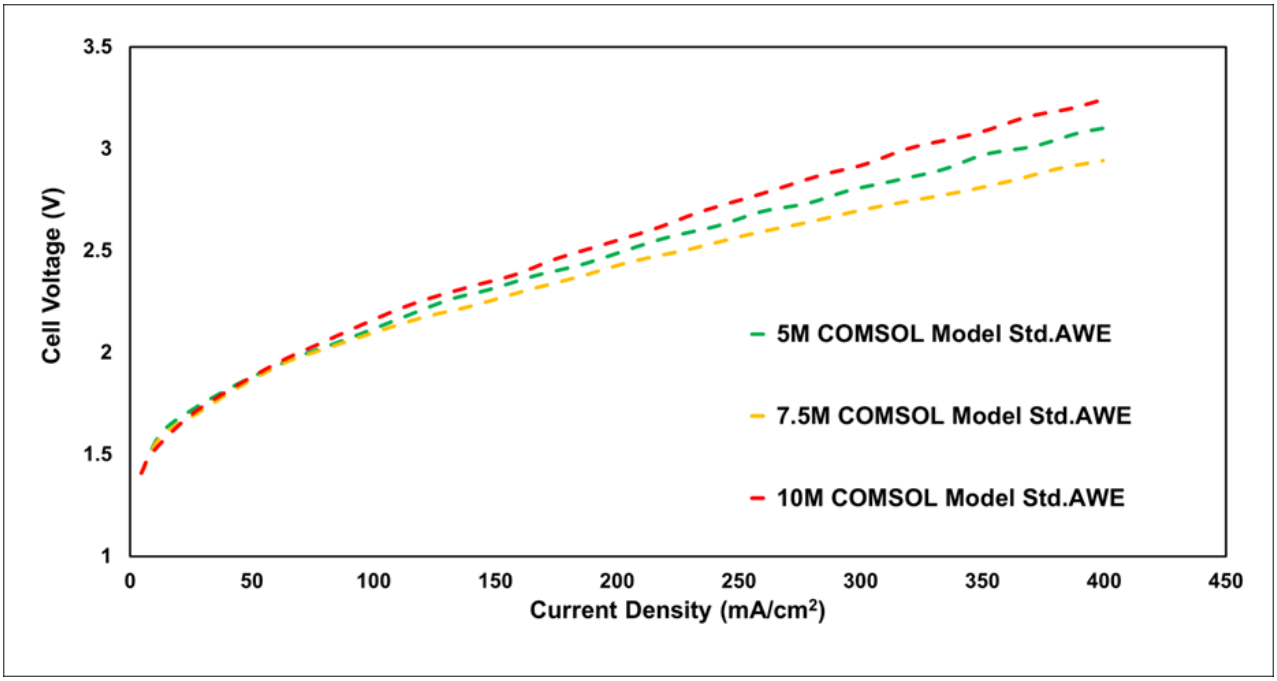

FIGURE 9 STANDARD NON-ZERO GAP ALKALINE ELECTROLYZER: POLARIZATION CURVE VARIATION AT DIFFERENT CELL ELECTROLYTE CONCENTRATIONS (5-10M "22-42 WT.%" KOH) AT 50°C, 10MM ELECTRODE DISTANCE.

When hydrogen (H_2) and oxygen (O_2) are produced, a biphasic mixture of gas and electrolyte is formed. The gas fraction in this mixture acts as a non-conductor, resulting in lower electrolyte conductivity, particularly in the vicinity of the electrodes. Bruggeman equation quantifies this effect, where an increase in the gas bubble fraction leads to a decrease in the electrolyte conductivity. Previous studies [14] have demonstrated that increasing electrolyte conductivity enhances electrolysis performance by reducing ohmic losses and consequently lowering the required energy. This highlights the significance of optimizing electrolyte conductivity to improve overall system efficiency. The model identifies an optimal electrolyte concentration at 32 wt. %

KOH, corresponding to a conductivity of 94.54 S/m at 50 °C [15]. Above this concentration, mass transfer limitations increases, while below it, the ohmic losses become excessively high due to the very low electrolyte conductivity[15]. Therefore, maintaining the electrolyte concentration within this optimum range is crucial for achieving efficient electrolysis performance. As shown in Figure 9, maintaining the electrolyte concentration within an optimum range (between 5-10 M) is crucial for achieving efficient electrolysis performance. The figure shows the variation in a performance metric, such as electrolysis efficiency or current density, as the electrolyte concentration is altered within the specified range as reported in[21].

3.7.3 Influence of Electrode-Diaphragm Distance

The ohmic overpotential in standard alkaline water electrolyzer cells is significantly influenced by the proximity of the electrode to the diaphragm. When the electrode-diaphragm distance is reduced, there is a smaller volume of electrolyte between these components, resulting in a decrease in the ohmic contribution from this compartment. This implies that the overall ohmic overpotential decreases with a shorter electrode-diaphragm distance. However, it is important to note that excessively narrow electrode-diaphragm distances can lead to a higher gas fraction during electrolysis. This increased gas fraction can significantly contribute to the ohmic overpotential, counteracting the benefits of reducing the distance. Consequently, it is reasonable to expect that there exists an optimal electrode-diaphragm distance that maximizes the performance of the alkaline water electrolyzer cell. Numerous studies have been conducted to calculate this optimum distance.

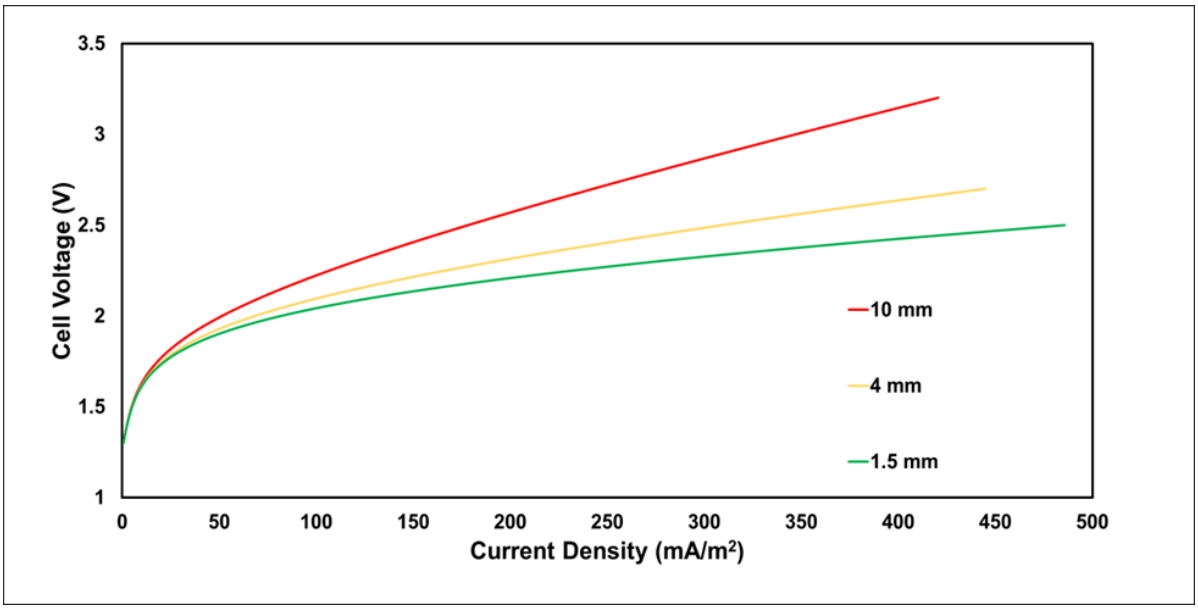

FIGURE 10 STANDARD NON-ZERO GAP ALKALINE ELECTROLYZER: POLARIZATION CURVE VARIATION AT DIFFERENT ELECTRODE-DIAPHRAGM DISTANCES (1.5-10 MM) AT 50°C, 32 WT.% KOH.

Figure 10 illustrates the polarization curves obtained from simulations when different electrode-diaphragm distances were considered, ranging from 1.5 mm to 10 mm, at a constant temperature of 50℃ and with a 32 wt—% KOH electrolyte concentration. The modeled curves show that as the distance between the electrode and the diaphragm decreases, the electrolysis potential also decreases.

3.7.4 Gas Generation Profile

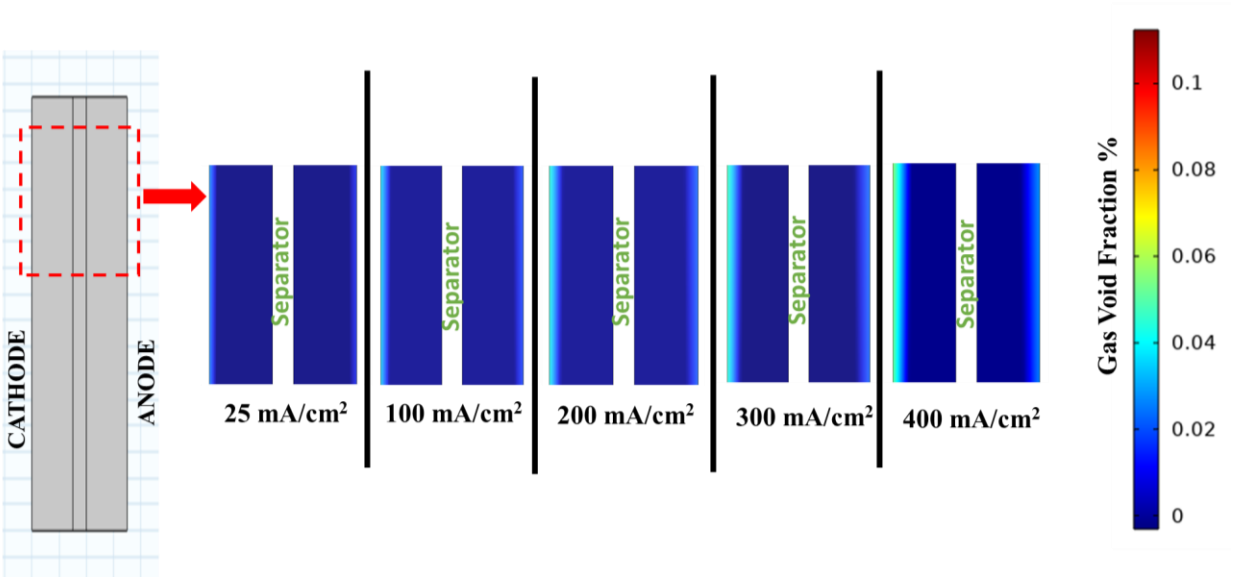

FIGURE 11 STANDARD ALKALINE ELECTROLYZER: DISPERSED PHASE FRACTION DISTRIBUTION IN HYDROGEN AND OXYGEN GAS COMPARTMENTS AT DIFFERENT CURRENT DENSITY VALUES.

Figure 11 depicts the changes in the gas profile as the current density varies within the alkaline water electrolyzer (AWE) cell. The void fractions of hydrogen and oxygen are presented, indicating the volume occupied by gas bubbles in each electrolytic chamber. The observed gas profile aligns with the familiar pattern near the electrode surface, consistent with findings from research published [14]. The dispersed phase fraction of gas bubbles exhibit a gradual increase from the bottom to the top of the electrode, primarily due to the accumulation of generated gas and the influence of the flow rate. This behavior has significant implications for the hydrodynamic characteristics of the biphasic flow in the alkaline water electrolyzer (AWE) cell. The presence of

gas bubbles plays a crucial role by creating a vertical curtain along the electrode surface, resulting in enhanced mixing and improved distribution of electrolyte species. This phenomenon contributes to more efficient mass transfer processes within the cell.

The findings presented in Figure 10 highlight the importance of managing gas bubble formation and distribution in the design and operation of AWE cells. A successful development of a 2D two-phase "Electrochemistry-Transport" coupled model for AWE was achieved. The model utilized an inhomogeneous Euler-Euler mixture modeling approach, allowing for the simulation of various operating conditions and simultaneous analysis of fluid dynamics and electrochemical phenomena. Efforts should be directed towards promoting efficient gas-liquid mixing and optimizing flow rates. By addressing these aspects, it is possible to enhance the overall performance and efficiency of the AWE cell, leading to improved electrolysis processes for hydrogen production.

3.8 Overpotential

The real cell voltage (U) exceeds the reversible voltage due to irreversibilities or overpotentials. Hence, the real cell voltage can be defined as the combined value of reversible voltage and overpotentials (η).

$$U = Urev + \sum \eta$$

The total overpotential is the sum of individual activation (η_{act}), ohmic (η_{ohm}), and concentration overpotentials (η_{conc}).

$$\sum\eta = \eta_{act} + \eta_{ohm} + \eta_{conc}$$

3.8.1 Activation Overpotential

The Butler-Volmer equation, in its simplified Tafel equation form, is a fundamental equation used to describe the electrochemical kinetics at the electrode/electrolyte interface. It relates the activation overpotential (η) to the current density (j) and the exchange current density (j0). The equation is based on the principles of chemical kinetics and electrochemical reactions.

The Tafel equation form of the Butler-Volmer equation is expressed as:

$$j = j0 * \exp\left(\frac{\alpha * F * \eta}{R * T}\right)$$

$$\eta_{actC} = 2.3 \cdot \frac{R \cdot T}{\alpha c \cdot F} \cdot \log\left(\frac{j}{j_o C}\right)$$

$$\eta_{actA} = 2.3 \cdot \frac{R \cdot T}{\alpha A \cdot F} \cdot \log\left(\frac{j}{j_o A}\right)$$

In this equation: j represents the actual current density in A/m², j0 represents the exchange current density in A/m², which is the current density at zero overpotential, α is the transfer coefficient (also known as symmetry factor), indicates the extent to which the electrochemical reaction occurs through charge transfer at the electrode-electrolyte interface. It represents the portion of the interfacial potential that helps reduce the free energy barrier during the reaction., F is the Faraday constant (96485 C/mol), representing the charge of one mole of electrons, R is the gas constant (8.314 J/(mol·K)), T is the absolute temperature in Kelvin, η represents the activation overpotential in volts (V).

In its Tafel equation form, the Butler-Volmer equation describes the relationship between the activation overpotential and the current density. It states that the current density exponentially depends on the activation overpotential, with the transfer coefficient, temperature, and exchange current density as additional influencing factors.

3.8.2 Ohmic Overpotential

Ohmic overpotential refers to the voltage drop caused by the electrical resistance encountered by the current as it passes through the electrodes, electrolyte, and membrane in an electrochemical system. It results from the resistance these components offer to the flow of electrical current. The electrical resistance of the electrodes, electrolyte, and membrane collectively contributes to the ohmic overpotential. The resistance is influenced by factors such as the conductivity, thickness, and geometries of these components. By considering the electrical resistance of each component, the ohmic overpotential can be estimated, providing valuable information about the losses incurred due to electrical resistance in the system. Managing and minimizing the ohmic overpotential is crucial for optimizing the efficiency and performance of electrochemical systems.

Electrode Resistance:

$$\sigma_{Ni} = \ 60000000 - 279650T + 532T^2 - 0.38057T^3$$

$$R_A = \frac{1}{\sigma_a}\left(\frac{L_a}{A_a}\right)$$

$$R_C = \frac{1}{\sigma_c}\left(\frac{L_c}{A_c}\right)$$

Electrolyte Resistance:

$$\sigma_{electrolyte} = -204.1 \cdot w - 0.28 \cdot w^2 + 0.5332 \cdot (w \cdot T) + 20720 \cdot \frac{w}{T} + 0.1043 \cdot w^3 - 0.00003 \cdot (w^2 \cdot T^2)$$

$$R_{\text{electrolyte}} = \frac{1}{\sigma_{\text{electrolyte}}} \left(\frac{d_{am}}{A_a} + \frac{d_{cm}}{A_c} \right)$$

Membrane Resistance:

$$R_{mem} = \frac{\delta_m \cdot \tau_m}{p_m \cdot \sigma_{\text{ele}} \cdot A_m}$$

Bubble Resistance:

$$\sigma_{eff-electrolyte} = \sigma_{electrolyte} \cdot \left(1 - \Phi_g\right)^{1.5}$$

$$R_{\text{eff- electrolyte}} = \frac{1}{\sigma_{\text{eff-electrolyte}}} \left(\frac{d_{am}}{A_a} + \frac{d_{cm}}{A_c} \right)$$

$$\eta_{ohm} = V_{ohm} = (R_C + R_A + R_{electrolyte} + R_{membrane} + R_{bubble}).I$$

3.8.3 Concentration Overpotential

Fick's law describes the flux of a species through a medium based on its concentration gradient. In the context of electrochemistry, it can be applied to calculate the concentration polarization or concentration overpotential at an electrode.

The concentration overpotential (η_{conc}) is related to the concentration gradient of a specific species (usually an electroactive species involved in the electrochemical reaction) near the electrode surface. It can be calculated using Fick's law, assuming that the diffusion of the species is the rate-limiting step and that the system is at steady-state:

$$\eta_{conc} = \left(\frac{RT}{nF}\right) * \ln\left(\frac{C_{bulk}}{C_{surface}}\right)$$

Where:

η_{conc} is the concentration overpotential,

R is the ideal gas constant (8.314 J/(mol·K)),

T is the temperature in Kelvin,

n is the number of electrons involved in the electrochemical reaction,

F is Faraday's constant (96485 C/mol),

C_bulk is the bulk concentration of the species, and

C_surface is the concentration of the species at the electrode surface.

Mass transfer layer width and effective diffusion coefficient were obtained from the literature sources [22,23].

Fick's law, at the electrode-electrolyte interface

$$\dot{n}_{O_2} = D_{eff}^{an} \frac{\left(C_{O_2,el} - C_{O_2,ch}\right)}{\delta_{an}}$$
$$\dot{n}_{H_2} = D_{eff}^{cat} \frac{\left(C_{H_2,el} - C_{H_2,ch}\right)}{\delta_{cat}}$$

$$C_{O_2,el}^{an} = C_{O_2,ch} + \frac{\delta_{an}\dot{n}_{O_2}}{D_{eff}^{an}}$$
$$C_{H_2,el}^{cat} = C_{H_2,ch} + \frac{\delta_{cat}\dot{n}_{H_2}}{D_{eff}^{cat}}$$

Resulting in contribution to the overpotential

$$V_{con} = \frac{R^*T}{2F} \ln \frac{C_{O_2,el}^{an}}{C_{O_2,0}^{an}} + \frac{R^*T}{2F} \ln \frac{C_{H_2,el}^{cat}}{C_{H_2,0}^{cat}}$$

3.9 Zero Gap Alkaline Water Electrolyzer

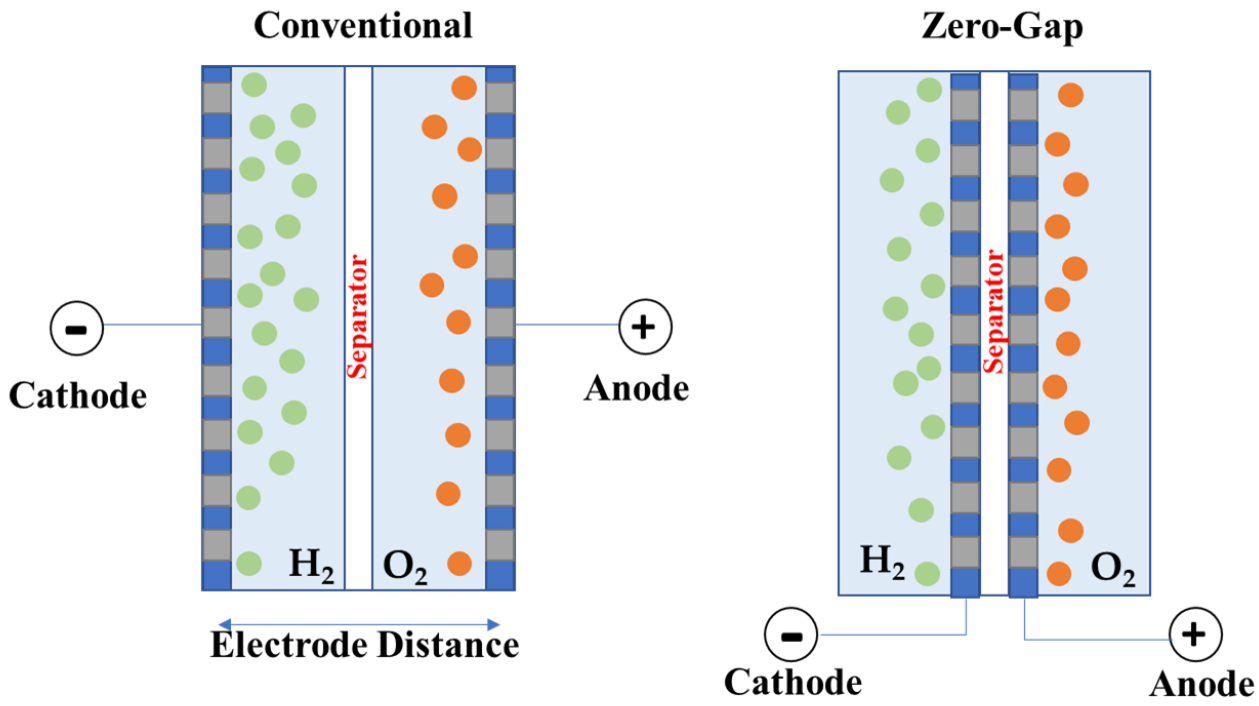

The zero-gap alkaline water electrolyzer (ZG-AWE) is an emerging technology with great potential for efficient and sustainable hydrogen production. In contrast to conventional alkaline electrolyzers, which typically employ a gap between the electrodes, the ZG-AWE eliminates this gap, improving performance and reducing energy consumption. The absence of a physical gap between the electrode and the separator allows for enhanced ionic conductivity and more efficient mass transport. Electrochemical reactions occur directly at the electrode surfaces, reducing ohmic losses and improving overall performance.

The modeling of zero-gap alkaline water electrolyzers (ZG-AWEs) has gained significant attention in recent years as it provides valuable insights into their performance and enables optimization for enhanced hydrogen production.

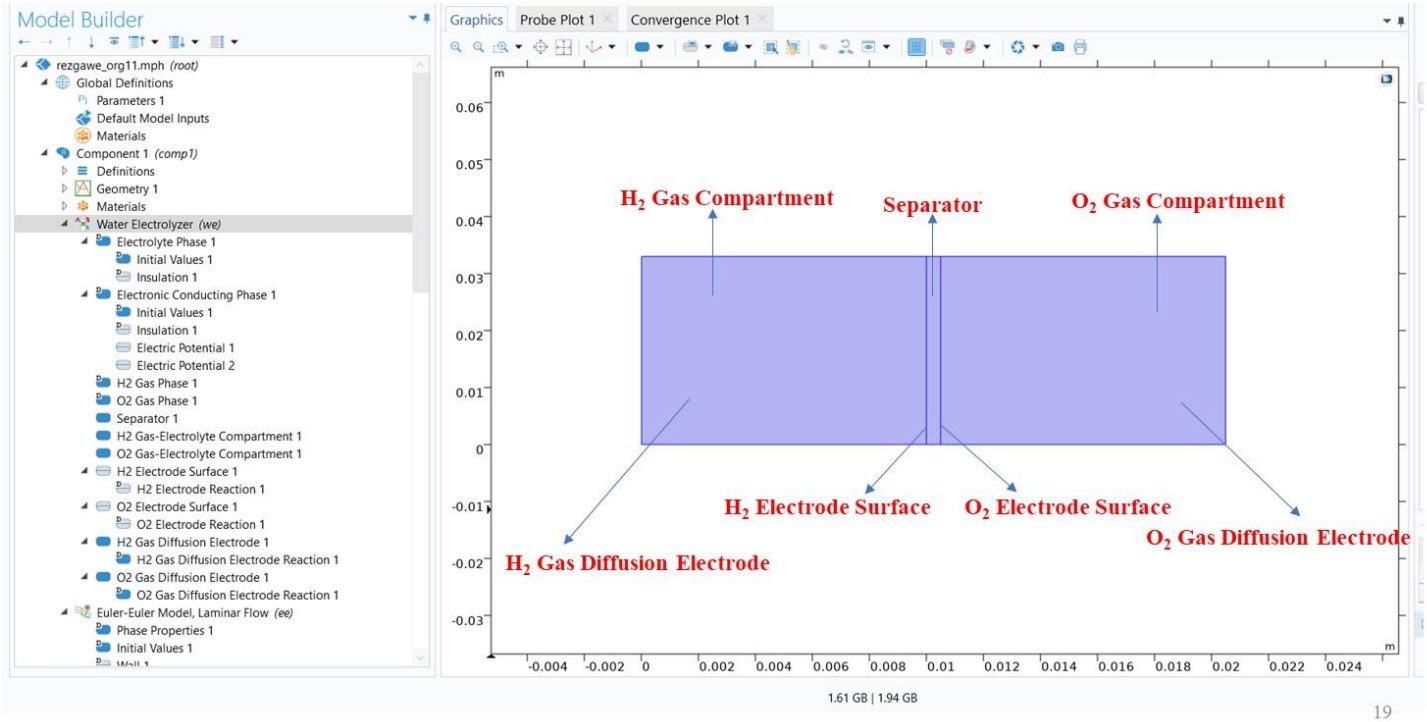

FIGURE 12 2D ZERO-GAP ALKALINE WATER ELECTROLYZER COMSOL MODEL.

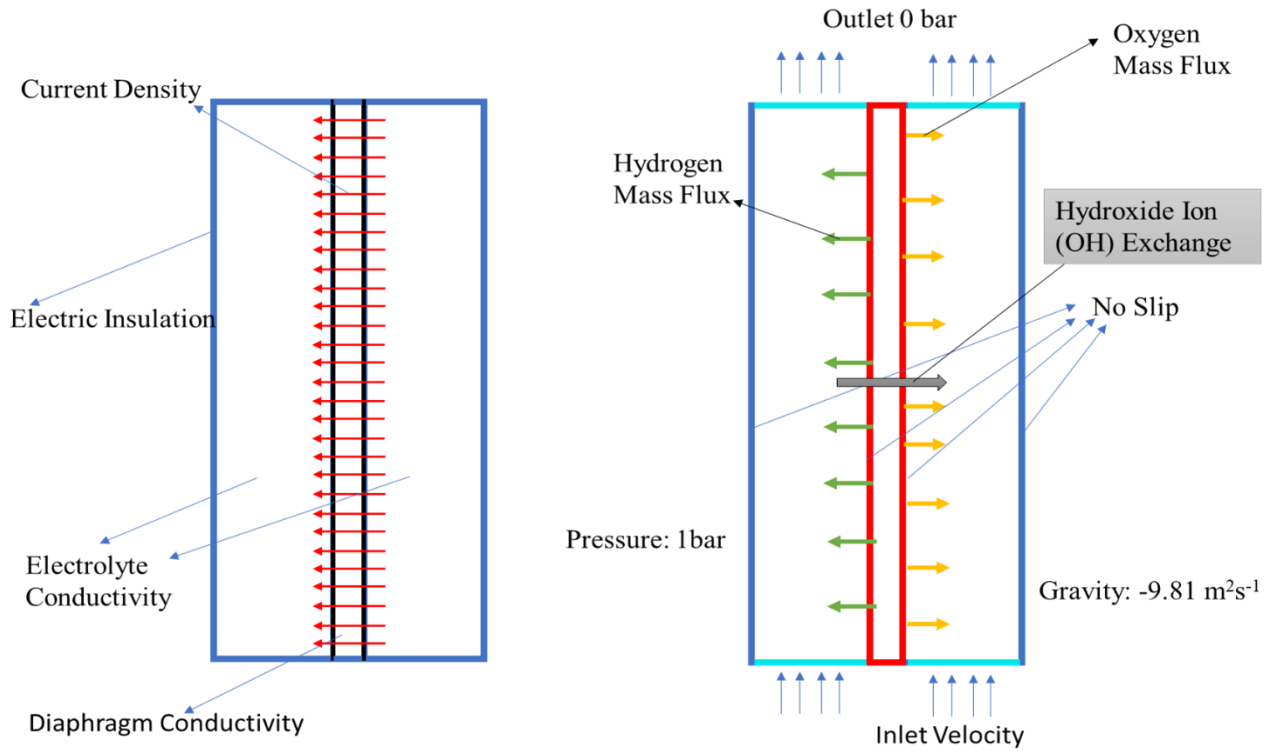

FIGURE 13 INITIAL AND BOUNDARY CONDITIONS FOR ZERO-GAP ALKALINE WATER ELECTROLYZER

3.9.1 Influence of Cell Temperature

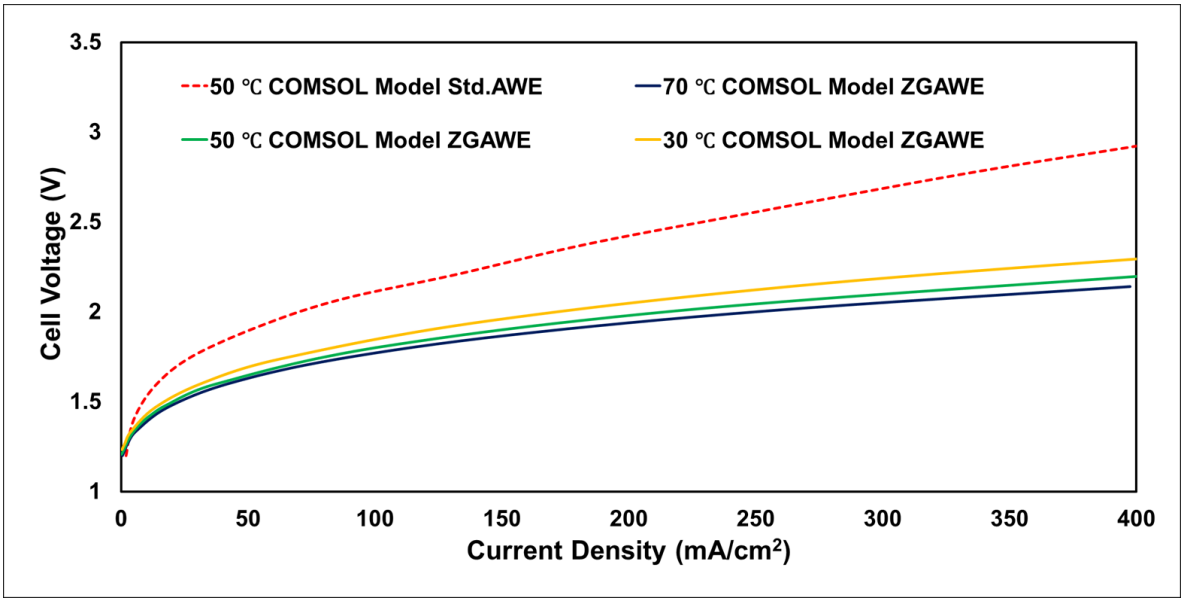

FIGURE 14* POLARIZATION CURVE SHOWING THE VARIATION WITH CELL TEMPERATURE *(30-70) °C AT 7.5 M (32 WT.%) KOH.

Figure 14 illustrates the polarization curve of a zero-gap alkaline water electrolyzer at different cell temperatures. As anticipated, the cell potential decreases as temperature increases, indicating improved favorable reaction free energies, and reduced reversible voltage. Furthermore, a notable reduction in overpotential is observed when comparing the standard alkaline water electrolyzer to the zero gap configuration at 50 ℃.

3.9.2 Gas Generation Profile

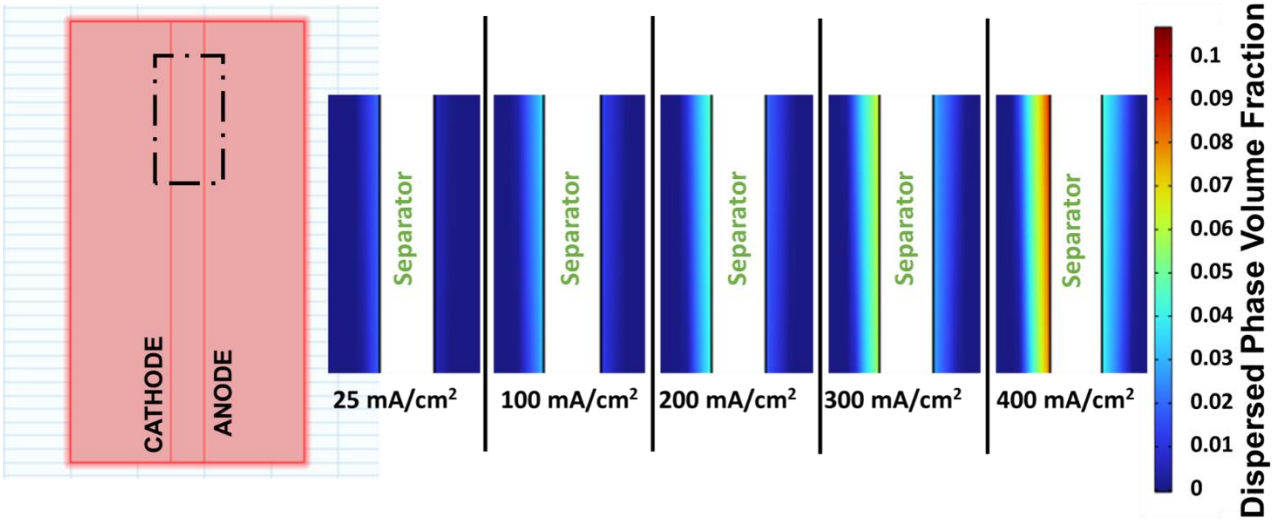

FIGURE 15 DISPERSED PHASE FRACTION DISTRIBUTION IN HYDROGEN AND OXYGEN GAS COMPARTMENTS AT DIFFERENT CURRENT DENSITY VALUES OF "ZERO-GAP ALKALINE ELECTROLYSIS CELL."

Figure 15 depicts the gas profile evolution in a zero-gap alkaline water electrolyzer (ZG-AWE) cell, showing the void fractions of hydrogen and oxygen. The gas fraction exhibits an upward trend within the electrode, gradually increasing from the bottom to the top. The observed behavior can be attributed to the accumulation of gas and the impact of variations in flow rate, which are due to the assumption of laminar flows in the models.

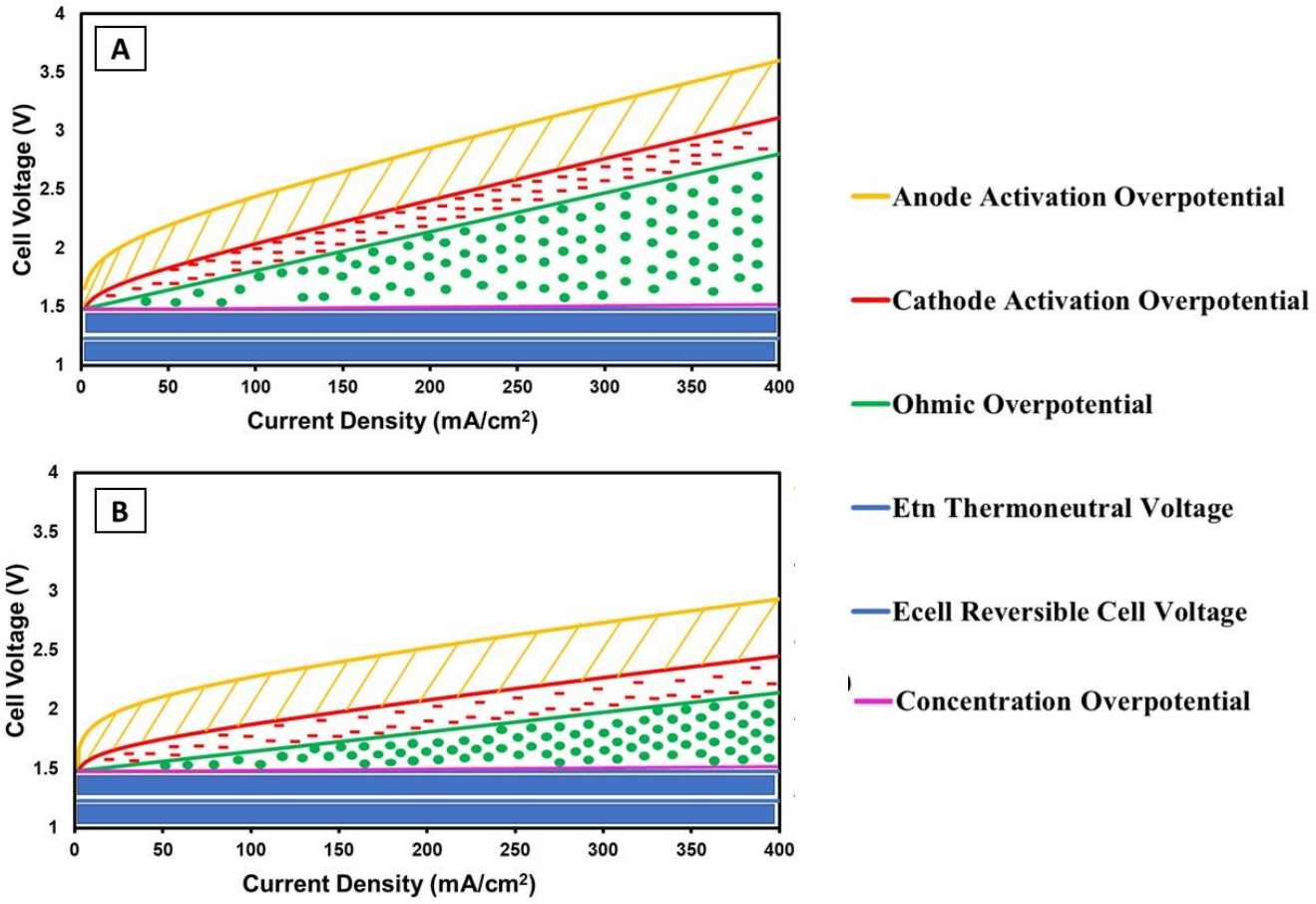

FIGURE 16 CONTRIBUTION OF ACTIVATION, OHMIC, AND CONCENTRATION OVERPOTENTIAL IN POLARIZATION CURVE FOR A) STD. ALKALINE WATER ELECTROLYZER AND B) ZERO-GAP ALKALINE WATER ELECTROLYZER AT 70 °C, 7.5 M (32 WT.%) KOH, 10MM ELECTRODE DISTANCE (STD. AWE).

Figure 16 provides a detailed analysis of the individual contributions of overpotential to the polarization curve in the context of alkaline water electrolyzers. The comparison is made between a standard alkaline water electrolyzer and a zero-gap alkaline water electrolyzer. The overpotential

refers to the additional voltage required to drive the electrochemical reactions at the electrode surfaces. The significant reduction in the ohmic overpotential of approximately 1.2 V observed in the zero gap configuration compared to the standard electrolyzer is noteworthy. The ohmic overpotential is attributed to the electrical resistance within the system, including the resistance of the electrodes, electrolyte, and other components. The electrical resistance is minimized by reducing the electrode-diaphragm distance to zero in the zero-gap configuration, resulting in a substantial decrease in the ohmic overpotential.

The polarization curve, which represents the relationship between the cell voltage and the current density, is a crucial characteristic of an electrolyzer. The individual contributions of overpotential to the polarization curve provide insights into the performance and efficiency of the electrolysis process. By analyzing Figure 13, it can be observed that the reduction in the ohmic overpotential significantly improves the overall performance of the zero-gap alkaline water electrolyzer compared to the standard configuration.

This finding highlights the advantages of employing the zero-gap configuration in alkaline water electrolyzers. The lower ohmic overpotential achieved in the zero-gap setup allows for operation at higher current densities, improving the electrolysis process's efficiency and performance. These results support the notion that careful design considerations, such as minimizing electrical resistance through innovative configurations, can greatly impact the performance of electrolyzers and enhance the overall efficiency of hydrogen production.

Chapter 4

Self-Terminating Electrodeposition of Platinum on Gold for PEMFC Electrodes

4.1 Experimental Methods and Materials

Potassium tetra chloroplatinate (K_2PtCl_4) with a purity of 99.99% trace metals basis and perchloric acid ($HClO_4$) with a purity of 70% (v/v) and 99.999% trace metal basis were procured from Merck. Loba Chemie Pvt Ltd provided 30% hydrogen peroxide (H_2O_2) with Extra Pure grade, containing less than 0.2% non-volatile matter and less than 0.05% sulphate content. Nitrogen (N_2) gas of N5.0 grade with a purity of 99.999% was used. Hydrochloric acid (HCl) with a purity of 35-38% (AR grade), nitric acid (HNO_3) with a purity of 69-72% (AR grade), potassium chloride (KCl) with AR grade, sodium hydroxide (NaOH) with AR grade, sulphuric acid (H_2SO_4) with AR grade, acetone (HPLC grade), and isopropyl alcohol (HPLC grade) were obtained from SD Fine Chemicals Ltd. For ICP-OES analysis, Fisher Scientific UK Ltd supplied hydrochloric acid (34-37%, Trace Metal grade) and nitric acid (67-69%, Trace Metal grade). Deionized water with a resistivity of 18 MΩ.cm from a Merck Milli-Q® unit was used in all experiments.

4.2 Electrochemical measurements

The electrochemical characterization was performed using a CH Instruments 608D potentiostat in a conventional three-electrode setup. The working electrode consisted of a rectangular strip of silicon measuring 30 mm x 3 mm, coated with a thin film of gold deposited through e-beam evaporation. These gold substrates were further coated with platinum overlayers, which were formed using the desired number of STED cycles. The exposed area of the platinum-coated electrodes ranged from 35 to 45 mm^2. For the reference electrode, an Ag(s)/AgCl(s)/KCl(aq) (1M) electrode obtained from CH Instruments, Inc. was utilized. A platinum foil electrode with a geometric surface area of 4 cm^2, sourced from Arora Matthey Limited and possessing a purity of over 99.99%, served as the counter electrode. All electrochemical data were reported using the IUPAC convention to ensure consistency, with all potential referenced against the Reversible Hydrogen Electrode (RHE). Currents were reported as density, representing the electrical current per unit geometric area (Acm^{-2}). The cleaning and pre-treatment procedures for the electrodes, glassware, and electrochemical cell followed the protocols described in [12]. These standardized protocols ensured the reliability and reproducibility of the experimental results obtained in this study.

ICP-OES Analysis: The quantification of platinum electrodeposited was performed using Inductively Coupled Plasma Optical Emission Spectroscopy (ICP-OES) with a Perkin Elmer Avio 200 instrument. The samples were subjected to leaching in aqua regia for 30 seconds. Subsequently, each sample was diluted to three different concentration levels (100x, 200x, and 500x). Calibration curves were generated using a blank solution and three known solutions of

K2PtCl4. The ICP-OES analysis enabled the determination of the amount of platinum present in the samples based on the measured emission intensities, providing accurate and reliable quantitative data.

4.3 Fabrication of platinum overlayers on gold substrates

The platinum electrodeposition process utilized an electrolyte comprising 3.0 mM K2PtCl4 as the platinum precursor and 0.5 M KCl as the supporting electrolyte. To achieve the desired pH of 4, HClO4 and NaOH were added to adjust the electrolyte's acidity. The platinum deposition profile was investigated using linear sweep voltammetry, following the method outlined in the study [11].

Specific potential levels were applied for the Self-Terminating Electrodeposition (STED) technique. The potential for platinum deposition was set at -0.42 V, while underpotential hydrogen (Hupd) desorption occurred at 0.78 V. A hold time of 30 seconds was maintained at each voltage level to ensure the proper deposition process, as shown in Figure 17 a.

Several studies were conducted to explore the platinum electrodeposition process further. Firstly, the variation in pH during electrodeposition was investigated to understand its impact on the process. Secondly, the relationship between pH and the number of electrodeposition cycles was examined to evaluate any correlation. Lastly, repeatability studies specifically focused on the electrodeposition of Pt with eight cycles onto Au substrates. Previous research conducted by our group focused on assessing the durability of platinum overlayers formed through self-terminating

electrodeposition. The results demonstrated that these thin films were capable of meeting the demanding criteria of retaining over 40% of their electrochemically active surface area (ECSA) after subjecting them to 30,000 cycles of ex-situ durability analysis. This durability is essential for their potential application in Fuel Cell Vehicles (FCVs). The successful synthesis of durable platinum films at the atomic layer level through electrodeposition represents a promising and cost-effective approach for manufacturing Proton Exchange Membrane Fuel Cells (PEMFCs)[11]. These investigations aimed to provide comprehensive insights into the behavior of the electrodeposition process and its potential effects on pH changes, cycle dependency, and repeatability.

To eliminate any dissolved oxygen from the electrolyte, the system was purged with nitrogen (N_2) gas for approximately 30 minutes before electrodeposition. Throughout the electrodeposition process, the headspace of the electrochemical cell was continuously purged with humidified N_2 gas. This purging helped prevent evaporation-induced platinum deposition at the liquid-gas interface, as outlined in reference[12].

After electrodeposition, the working electrode was carefully removed from the electrochemical cell, rinsed with deionized (DI) water, and dried using a stream of N_2 gas. These post-electrodeposition steps ensured the cleanliness and integrity of the synthesized samples for subsequent analysis and characterization.

4.4 Chronoamperometry

The conversion of charge under the platinum reduction peak to the mass of platinum reduction can be accomplished using Faraday's law of electrolysis. Faraday's law states that the amount of substance produced or consumed during an electrolysis process is directly proportional to the quantity of electric charge passed through the electrolyte.

The equation for Faraday's law is given by:

$$m = \frac{Q * M}{n * F}$$

Where:

m is the mass of the substance (in this case, platinum) being deposited or reduced,

Q is the total electric charge passed through the electrolyte during the reduction process,

M is the molar mass of platinum,

n is the number of electrons involved in the reduction reaction (which can be determined from the balanced chemical equation),

F is Faraday's constant (approximately 96,485 C/mol).

$$1\ \mu g\ cm^{-2} = (10^{-6} g/(195.08\ g\ mole\ of\ Pt)) * (96{,}485\ C/1\ mole\ of\ e^{-})$$
$$* (96{,}485\ C/1\ mole\ of\ e^{-}) * (2\ mole\ of\ e^{-}/1\ mole\ of\ Pt) * (10^{3} mC/1\ C)$$
$$1\ \mu g\ cm^{-2} = 0.99\ \text{mC}\ cm^{-2}$$

To calculate the mass of platinum reduced during the electrolysis process, one must determine the total electric charge passed during the reduction peak, calculated from the area under the curve of chronoamperometry profiles. The mass of platinum is obtained by substituting these values into the equation above and considering the number of electrons (2 electrons) involved in the reduction reaction.

Study 1: Variation in pH during Electrodeposition

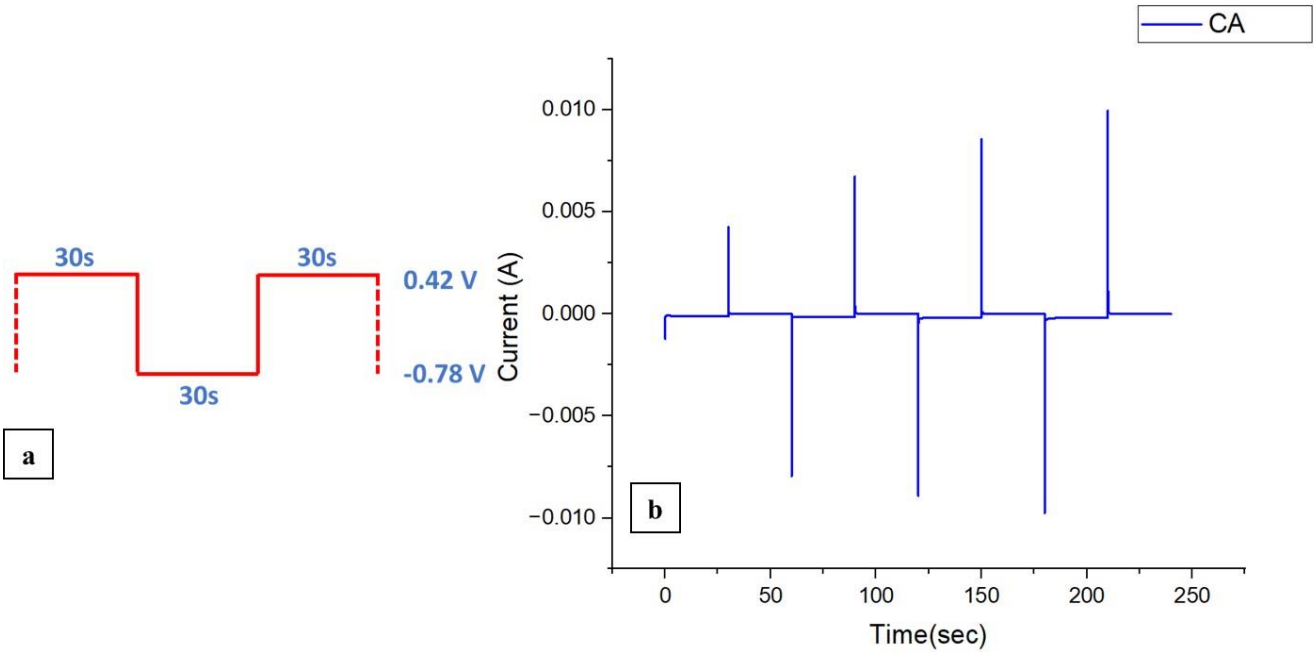

FIGURE 17 (A) POTENTIAL SCHEME APPLIED FOR STED, (B) CA PROFILES FOR FOUR CYCLES OF PT DEPOSITION.

TABLE 3 VARIATION IN PH DURING8 CYCLE STED OF PT ON AU

Sample No	pH (Before Electrodeposition)	pH (After Electrodeposition)
1	4.01	4.01
2	4.01	4
3	4	4
4	4	4

Study 2: Relationship between pH and the number of electrodeposition cycles

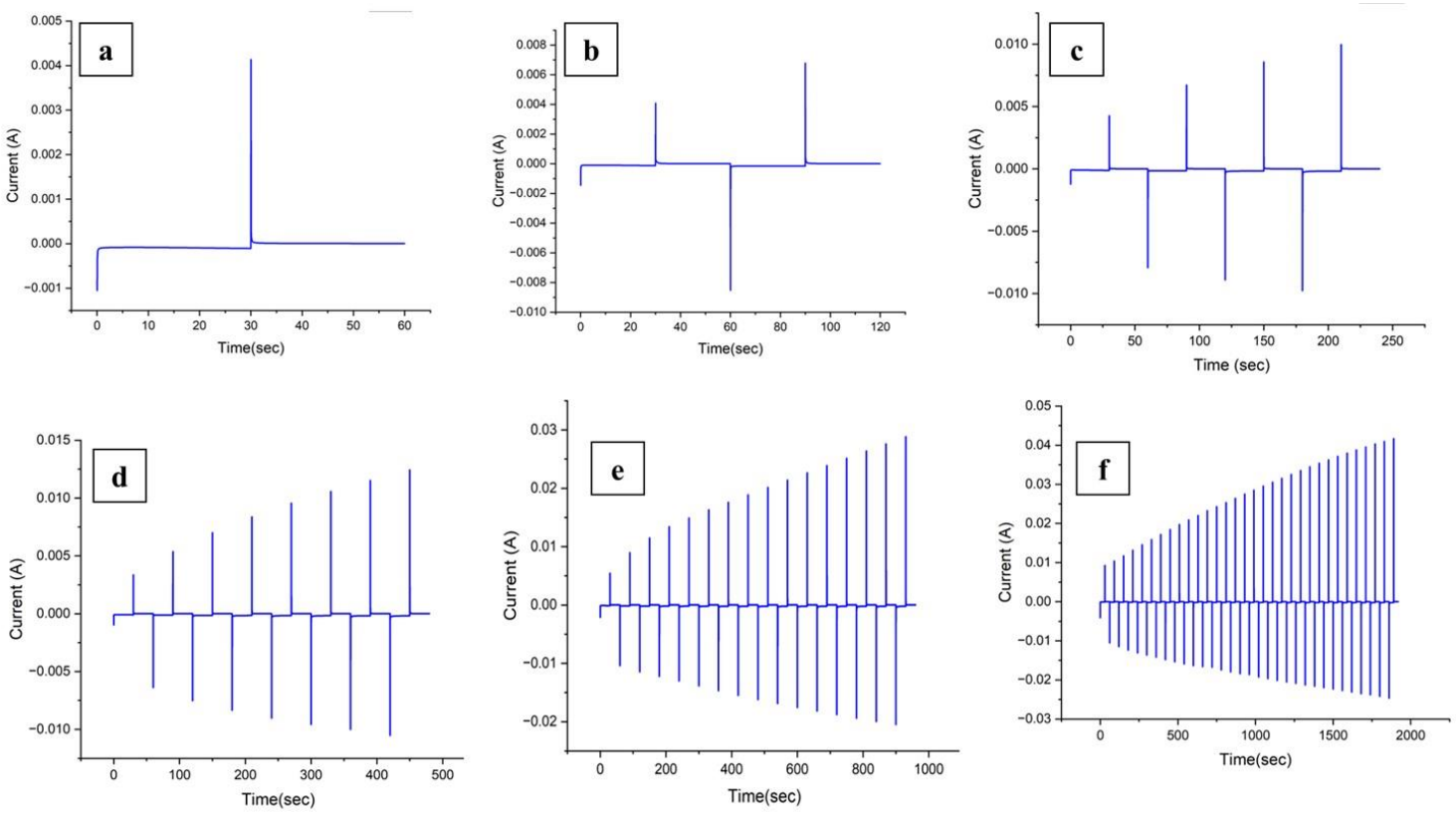

FIGURE 18 CA PROFILES FOR 1,2,4,8,16,32 (A-F) CYCLES OF PT DEPOSITION.

Study 1 investigated the potential variation in pH during the electrodeposition of platinum on gold using the 4-cycle self-terminating electrodeposition process. This study aimed to assess whether the electrodeposition process had any significant impact on the pH of the electrolyte. The results of Study 1 revealed that the pH remained unchanged throughout the electrodeposition process. This indicates that the electrochemical reactions involved in the deposition of platinum did not cause any noticeable shifts in the acidity or alkalinity of the electrolyte.

Study 2 examined the influence of the number of electrodeposition cycles on pH changes. The objective was to determine whether the pH of the electrolyte varied with an increasing number of electrodeposition cycles. The findings of study 2 indicated that even as the number of electrodeposition cycles increased, the pH remained constant. This suggests that the electrodeposition process, including multiple cycles, did not significantly alter the pH of the electrolyte.

The consistent pH observed in both studies is beneficial as it ensures a stable electrochemical environment throughout the electrodeposition process. This stability can contribute to the reproducibility and reliability of the produced platinum-gold composite material.

TABLE 4 ESTIMATED PT LOADING FROM CA AND ICP-OES ANALYSIS

Sample No	Area Under I-t Curve CA (mC)	Area of Working Electrode (cm^2)	Pt Deposition Charge per Area (mC/cm^2)	Amount of Pt Deposited ($\mu g/cm^2$)	Amount of Pt Deposited from ICP-OES analysis. ($\mu g/cm^2$)
S2	2.98	0.60	4.96	5.01	4.5 $\pm$ *0.5*
S3	2.81	0.64	4.39	4.44	3.5 $\pm$ *0.7*
S4	3.01	0.70	4.3	4.34	3.3 $\pm$ *1.1*
S5	2.47	0.60	4.12	4.16	3.1 $\pm$ *0.9*
S6	2.046	0.63	3.35	3.38	3.5 $\pm$ *1.0*

Study 3: Repeatability studies specifically focused on the electrodeposition of Pt with eight cycles onto Au substrates.

Table 4 compares the estimated platinum (Pt) loading obtained from the chronoamperogram and the loading measured using Inductively Coupled Plasma Optical Emission Spectroscopy (ICP-OES). The platinum loading corresponding to a complete monolayer coverage of the projected area is evaluated 3.3 $\mu g/cm^2$. The Pt loading is determined by correlating the difference in charge

between anodic and cathodic currents in the chronoamperogram with the amount of platinum deposited in each cycle using Faraday's law of electrolysis. The repeatability studies focused on Pt electrodeposition with eight cycles onto Au substrates, and the results, as shown in Table 5, demonstrate that the deposition process was consistent, yielding a loading range of approximately 3-5 $\mu g/cm^2$.

In conclusion, this research focused on the self-terminating electrodeposition of platinum on gold substrates for potential application in proton exchange membrane fuel cell (PEMFC) electrodes. The experimental methods and materials were carefully selected to ensure accurate and reliable results. The electrodeposition process was performed using a specific electrolyte composition, and the pH of the electrolyte was adjusted to 4 using $HClO_4$ and NaOH. Linear sweep voltammetry was employed to analyze the platinum deposition profile. The self-terminating electrodeposition (STED) technique involved specific potential levels and a hold time of 30 seconds at each voltage level. Several studies were conducted to gain insights into the electrodeposition process. Study 1 investigated the potential variation in pH during the electrodeposition of platinum on gold, and the results indicated that the pH remained unchanged throughout the process. Study 2 examined the influence of the number of electrodeposition cycles on pH changes and revealed a consistent pH regardless of the number of cycles. ICP-OES analysis was utilized to quantify the amount of platinum electrodeposited. The estimated Pt loading from chronoamperogram and ICP-OES measurements were compared, and the results showed a consistent and reproducible deposition process, yielding loading levels of approximately 3-5 $\mu g/cm^2$. Overall, the research provided valuable insights into the self-terminating electrodeposition process of platinum on gold substrates. The findings demonstrated the stability of pH during the electrodeposition and highlighted the

repeatability of the process with a consistent Pt loading. These results contribute to the understanding and potential of applying platinum-gold composite materials in PEMFC electrodes, enhancing their performance and reliability.

.

Chapter 5

Conclusion

In conclusion, electrolytic hydrogen production using Alkaline Water Electrolysis (AWE) offers significant advantages in terms of energy density and storage capabilities. However, traditional AWE systems face limitations due to high internal resistance, restricting their operation to low current densities. The Zero Gap configuration of AWE (ZGAWE) addresses this issue by reducing ohmic overpotential and enabling higher current densities, resulting in improved efficiency. This study successfully developed a 2D, 2 phase electrochemistry-transport coupled model of the ZGAWE cell using COMSOL Multiphysics. The model incorporated fluid dynamics and electric current conservation equations, utilizing the Euler-Euler approach to describe the two-phase bubbly flow. Experimental validation and comparative studies were conducted with a standard non-zero gap alkaline electrolyzer, revealing a significant reduction in the ohmic overpotential by approximately 0.8 volts by modeling both standard and zero gap configurations.

On a separate note, the research investigated the electrodeposition of platinum on gold substrates for potential use in Proton Exchange Membrane Fuel Cell (PEMFC) electrodes. By employing a specific electrolyte composition with pH four and utilizing linear sweep voltammetry and self-terminating electrodeposition techniques, multiple studies were conducted to examine pH variations, electrodeposition cycles' influence, and platinum deposition quantification. The results demonstrated stable pH levels throughout the process, consistent pH regardless of cycle number, and reproducible deposition with 3-5 $\mu g/cm^2$ loading levels. These findings significantly

contribute to our understanding and application of platinum-gold composites in optimizing the performance and reliability of PEMFC electrodes.

Future Scope

Developed a two-dimensional two-phase "Electrochemistry-Transport" coupled model for alkaline water electrolyzers using an inhomogeneous Euler-Euler mixture modeling approach. The model demonstrated high versatility in simulating various operating conditions while simultaneously analyzing fluid dynamics and electrochemical phenomena. It revealed that the generated gases create a "curtain profile" within the electrode, leading to increased void fraction vertically due to gas accumulation. Additionally, the model confirmed a reduction in ohmic overpotential with the Zero Gap configuration compared to the standard AWE setup. Future work will involve visualizing membrane leaks in alkaline water electrolyzers and modeling the entire electrolyzer system with a gas-liquid separator. The study on self-terminated electrodeposition of platinum on gold revealed several key findings. The pH levels remained stable throughout the electrodeposition process, indicating a consistent and controlled environment. Secondly, regardless of the cycle number, the pH levels remained consistent, indicating the repeatability of the electrodeposition process. Lastly, the deposition achieved loading levels of 3-5 $\mu g/cm^2$, demonstrating the reproducibility of the method. In future work, the focus will be on developing a flow cell setup to enable continuous electrodeposition. This will allow for a continuous and uninterrupted electrodeposition process, providing more efficient and scalable production of platinum overlayers. By implementing a flow cell setup, it will be possible to scale up the electrodeposition process to meet larger production demands and explore its application in various fields.

Bibliography

[1] D. Huang, B. Xiong, J. Fang, K. Hu, Z. Zhong, Y. Ying, X. Ai, Z. Chen, A multiphysics model of the compactly-assembled industrial alkaline water electrolysis cell, Appl. Energy. 314 (2022) 118987. https://doi.org/10.1016/j.apenergy.2022.118987.

[2] M.R.M. Cruz, D.Z. Fitiwi, S.F. Santos, J.P.S. Catalão, A comprehensive survey of flexibility options for supporting the low-carbon energy future, Renew. Sustain. Energy Rev. 97 (2018) 338–353. https://doi.org/10.1016/j.rser.2018.08.028.

[3] M. Ball, M. Weeda, The hydrogen economy - Vision or reality?, Int. J. Hydrogen Energy. 40 (2015) 7903–7919. https://doi.org/10.1016/j.ijhydene.2015.04.032.

[4] A.Z. Arsad, M.A. Hannan, A.Q. Al-Shetwi, M. Mansur, K.M. Muttaqi, Z.Y. Dong, F. Blaabjerg, Hydrogen energy storage integrated hybrid renewable energy systems: A review analysis for future research directions, Int. J. Hydrogen Energy. 47 (2022) 17285–17312. https://doi.org/10.1016/j.ijhydene.2022.03.208.

[5] F. Zhang, P. Zhao, M. Niu, J. Maddy, The survey of key technologies in hydrogen energy storage, Int. J. Hydrogen Energy. 41 (2016) 14535–14552. https://doi.org/10.1016/j.ijhydene.2016.05.293.

[6] S. Sharma, S.K. Ghoshal, Hydrogen the future transportation fuel: From production to applications, Renew. Sustain. Energy Rev. 43 (2015) 1151–1158. https://doi.org/10.1016/j.rser.2014.11.093.

[7] Q. Feng, X.Z. Yuan, G. Liu, B. Wei, Z. Zhang, H. Li, H. Wang, A review of proton exchange membrane water electrolysis on degradation mechanisms and mitigation strategies, J. Power Sources. 366 (2017) 33–55. https://doi.org/10.1016/j.jpowsour.2017.09.006.

[8] S. Pedram, M. Batool, K. Yapp, L. Bonville, J. Jankovic, A Review on Bioinspired Proton Exchange Membrane Fuel Cell: Design and Materials, Adv. Energy Sustain. Res. 2 (2021) 2000092. https://doi.org/10.1002/aesr.202000092.

[9] Y. Liu, H. You, Y.C. Kimmel, D. V. Esposito, J.G. Chen, T.P. Moffat, Self-terminating electrodeposition of Pt on WC electrocatalysts, Appl. Surf. Sci. 504 (2020) 144472. https://doi.org/10.1016/j.apsusc.2019.144472.

[10] Y. Liu, D. Gokcen, U. Bertocci, T.P. Moffat, Self-terminating growth of platinum films by electrochemical deposition, Science 80 (2012) 1327–1330. https://doi.org/10.1126/science.1228925.

[11] K. Agrawal, S. Chaudhary, D. Parvatalu, V. Santhanam, Durability of Platinum Overlayers formed By Self-Terminating Electrodeposition, ECS Meet. Abstr. MA2021-02 (2021) 1164–1164. https://doi.org/10.1149/ma2021-02391164mtgabs.

[12] K. Agrawal, A.A. Naik, S. Chaudhary, D. Parvatalu, V. Santhanam, Prudent Practices in

ex situ Durability Analysis Using Cyclic Voltammetry for Platinum-based Electrocatalysts, Chem. - An Asian J. 16 (2021) 3311–3325. https://doi.org/10.1002/asia.202100746.

[13] D. Le Bideau, P. Mandin, M. Benbouzid, M. Kim, M. Sellier, F. Ganci, R. Inguanta, Eulerian two-fluid model of alkaline water electrolysis for hydrogen production, Energies. 13 (2020) 1–14. https://doi.org/10.3390/en13133394.

[14] A. Zarghami, N.G. Deen, A.W. Vreman, CFD modeling of multiphase flow in an alkaline water electrolyzer, Chem. Eng. Sci. 227 (2020) 115926. https://doi.org/10.1016/j.ces.2020.115926.

[15] J. Rodríguez, E. Amores, Cfd modeling and experimental validation of an alkaline water electrolysis cell for hydrogen production, Processes. 8 (2020) 1–17. https://doi.org/10.3390/pr8121634.

[16] M. Li, Q. Ma, W. Zi, X. Liu, X. Zhu, S.F. Liu, Pt monolayer coating on complex network substrate with high catalytic activity for the hydrogen evolution reaction, Sci. Adv. 1 (2015) 1–8. https://doi.org/10.1126/sciadv.1400268.

[17] L. Pang, M. Li, Q. Ma, Y. Zhang, X. Ren, D. Zhang, S.F. Liu, Controlled Pt Monolayer Fabrication on Complex Carbon Fiber Structures for Superior Catalytic Applications, Electrochim. Acta. 222 (2016) 1522–1527. https://doi.org/10.1016/j.electacta.2016.11.134.

[18] Y.J. Deng, V. Tripkovic, J. Rossmeisl, M. Arenz, Oxygen Reduction Reaction on Pt Overlayers Deposited onto a Gold Film: Ligand, Strain, and Ensemble Effect, ACS Catal. 6 (2016) 671–676. https://doi.org/10.1021/acscatal.5b02409.

[19] J. Byun, S.H. Ahn, J.J. Kim, Self-terminated electrodeposition of platinum on titanium nitride for methanol oxidation reaction in acidic electrolyte, Int. J. Hydrogen Energy. 45 (2020) 9603–9611. https://doi.org/10.1016/j.ijhydene.2020.01.204.

[20] MPMG Weijs, L.J.J. Janssen, G.J. Visser, Ohmic resistance of solution in a vertical gas-evolving cell, J. Appl. Electrochem. 27 (1997) 371–378. https://doi.org/10.1023/A:1018449301423.

[21] J. Brauns, T. Turek, Alkaline water electrolysis powered by renewable energy: A review, Processes. 8 (2020). https://doi.org/10.3390/pr8020248.

[22] MT de Groot, A.W. Vreman, Ohmic resistance in zero gap alkaline electrolysis with a Zirfon diaphragm, Electrochim. Acta. 369 (2021). https://doi.org/10.1016/j.electacta.2020.137684.

[23] J. Lee, A. Alam, C. Park, S. Yoon, H. Ju, Modeling of gas evolution processes in porous electrodes of zero-gap alkaline water electrolysis cells, Fuel. 315 (2022) 123273. https://doi.org/10.1016/j.fuel.2022.123273.